Bioorganic Chemistry 166 (2025) 109167

IMPACT FACTOR : 4.7
Q1

Contents lists available at ScienceDirect

Bioorganic Chemistry

journal homepage: www.elsevier.com/locate/bioorg

Design, synthesis, bioactivity evaluation, and molecular modeling of pyridin-2-yl-pyrimidine: Potential Antimicrobial and anti-tuberculosis agents

Xue Xia [a], Jian Shen [b], Jindong Dai [b], Koshika Arumuagam [c], Kanagaraj Rajalakshmi [b], Yuvaraj Dinakarkumar [d], Panneerselvam Theivendren [e,*], Selvaraj Muthusamy [b,*], Dongwei Zhu [b,*], Haodong Yuan [a,*]

[a] Department of Clinical Laboratory, Zhangjiagang Hospital affiliated to Soochow University, Zhangjiagang, Jiangsu 215600, PR China
[b] Department of Immunology, Jiangsu Key Laboratory of Laboratory Medicine, School of Medicine, School of Chemistry and Chemical Engineering, Jiangsu University, Zhenjiang 212013, PR China
[c] Department of Chemistry, School of Sciences, Vels Institute of Science, Technology & Advanced Studies, Pallavaram, Chennai, Tamil Nadu 600117, India
[d] Department of Biotechnology, School of Life Sciences Chennai, Vels Institute of Science, Technology and Advanced Studies (VISTAS), Tamil Nadu, India
[e] Department of Pharmaceutical Chemistry & Analysis, School of Pharmaceutical Sciences, Vels Institute of Science, Technology & Advanced Studies, Pallavaram, Chennai, Tamil Nadu 600117, India

ARTICLE INFO

Keywords:
Fused pyrimidines
Anti-tuberculosis
Gram-positive
Gram-negative and fungal strains

ABSTRACT

The rise in antimicrobial resistance has underscored the urgent need for novel therapeutic agents. Pyrimidine derivatives, known for their broad-spectrum antimicrobial activity, have emerged as promising candidates. A new series of fused pyrimidine-5-carbonitrile derivatives were synthesized and evaluated for their antibacterial, antifungal, and anti-tuberculosis (anti-TB) activities. Molecular docking studies were conducted to assess their binding affinity with the InhA enzyme, a key component in bacterial fatty acid synthesis, and compared their effectiveness to Ciprofloxacin. These compounds were synthesized using standard organic methods and characterized by NMR, mass spectrometry, and other spectroscopic techniques. Antibacterial and antifungal activities were evaluated using the agar well-diffusion and cup-plate agar diffusion methods, respectively. Anti-TB activity was assessed against the MTB H37Ra strain using the Resazurin assay. The Minimum Inhibitory Concentration (MIC) values ranged from 10.6 to 17.8 μg/mL, indicating potent antibacterial activity, particularly against both Gram-positive and Gram-negative bacteria for compounds **2a1, 2a3** and **2a20**. Structural-activity relationship (SAR) studies revealed that lipophilic and electron-withdrawing groups enhanced antimicrobial potency. The promising results of compounds 2a1 and 2a20 highlight their potential as lead candidates in the development of new antimicrobial and anti-TB therapies.

1. Introduction

The World Health Organization (WHO) has recognized antibacterial drug resistance as a substantial worldwide public health issue. This is especially accurate for infections caused by antibiotic-resistant strains of *Enterococcus faecium*, Methicillin Resistant *Staphylococcus aureus*, *Klebsiella pneumoniae*, and *Acinetobacter baumannii* [1,2]. Hence, there is an ongoing need to create innovative antibacterial substances that explicitly focus on recognized and scientifically proven objectives, while also displaying resilience against current resistance mechanisms. InhA is a bacterial type topoisomerase IIA protein, and an established target of a range of antibacterial drugs, including fluoroquinolones like Nalidixic acid (I) and Ciprofloxacin (II) [1,3]. These drugs attach to the DNA-enzyme complex and enhance its stability in the cleaved form, therefore, preventing DNA replication, and ultimately causing bacterial cell death [4]. Although the use of this category of drug has been effective over time in treating bacterial infections, they are now facing resistance because of the changes that occur to the identity of their molecular targets [5–7]. Therefore, the current and future research efforts in the area seek to provide drugs that are not only effective in fighting drug-

* Corresponding authors.
E-mail addresses: tpsphc@gmail.com (P. Theivendren), rajselva311@ujs.edu.cn (S. Muthusamy), 1000005601@ujs.edu.cn (D. Zhu), hdyuan0920@163.com (H. Yuan).

https://doi.org/10.1016/j.bioorg.2025.109167
Received 10 August 2025; Received in revised form 19 October 2025; Accepted 26 October 2025
Available online 28 October 2025

resistant strains of bacteria, but also possess improved properties concerning absorption, distribution, metabolism and excretion within the body in addition to their safety profile [8]. Pharmaceutical firms have recently discovered new forms of bacterial topoisomerase IIA inhibitors (NBTIs) that are distinct from fluoroquinolones [9]. Two examples of these inhibitors are Gepotidacin and Zoliflodacin and these inhibitors have successfully completed phase II clinical studies for the treatment of *Neisseria gonorrhoeae* infections that to Zoliflodacin has been designated for an International Phase III study [10,11]. Moreover, pyrimidine and fused pyrimidine serve as a fundamental structure for a wide range of antimicrobial medications, such as Essramycin is a newly developed antibiotic that is obtained from marine *Streptomyces* species [12] and it falls within the category of antibiotics known as 1,2,4-triazolo[1,5-*a*] pyrimidine. The pyrimidine and fused pyrimidine have antibacterial efficacy against both Gram-positive and Gram-negative bacteria, as shown by its MIC [13–17]. Pyrimidine derivatives are known to display potent antimicrobial and TB (tetra-butyl) activities because they are structurally similar to nucleic acid bases so can inhibit microbial DNA and enzyme function. They share the benefits of extensive spectrum of activity with Gram-positive and Gram-negative bacteria and against drug-resistant *Mycobacterium tuberculosis* isolates. Pyrimidine scaffolds can undergo a variety of structural modification to enhance potency and selectivity. Moreover, they possess good pharmacokinetic behavior including high bioavailability, metabolic stability and this makes them appealing drug development candidates. But pyrimidine drugs are not without faults. Derivatives are very poisonous and cause side effects to host cells. Poor bioavailability and solubility may restrict their biological use. Nevertheless, pyrimidine-based compounds remain an important region of interest in drug discovery both as antimicrobial and anti-TB agents, and optimization is still being studied. This was an attempt to have a highly effective anti-TB drug based on the earlier significance of pyrimidine and fused pyrimidines. Besides this, a number of designed pyrimidine derivatives were also examined with molecular docking studies to determine what their binding mechanisms in the active area were. Thereafter, the analysis was conducted to find out the mechanism of action of the most potent synthetic drugs and they can act as InhA inhibitors.

2. Materials and methods

2.1. Materials

The chemical reagents and solvents were sourced from Sigma Aldrich, a company based in Germany. Thin-layer chromatography (TLC) was used to monitor and document the reactions. The plastic sheets were pre-coated with a 0.2 mm silica gel layer containing a vivid indicator from E. Merck. Melting points were measured with a Stuart electrothermal melting point apparatus and were stable. The infrared spectra were recorded by analyzing potassium bromide (KBr) discs with a Bruker spectrophotometer made in Mumbai, India. The ^{1}H and ^{13}C nuclear magnetic resonance (NMR) spectra were obtained using a Bruker instrument operating at 400 MHz (MHz) in Mumbai, India. Mass spectrometry data was collected with a Shimadzu GC MS QP 5000 quadrupole mass spectrometer located in Chennai, India. TMS was the internal reference, and chemical shifts were measured in parts per million (ppm) with DMSO-d_6 or CDCl3 as solvents. The VARIO-Elementer equipment was employed for elemental analysis of carbon (C), hydrogen (H), and nitrogen (N) samples from Mumbai, India.

2.2. Methods

2.2.1. Target identification

Several bioinformatic tools were then used for systematic identification of potential MTB targets and evaluation of the related synthetic drug candidates, GeneCards, OMIM, Swiss Target Prediction, g:Profiler and ShinyGO. For genetic and disease related information, GeneCards and OMIM (Online Mendelian Inheritance in Man) were consulted and the Swiss Target Prediction platform was utilized to predict interactions between the isolated compounds and their potential biological target. g: Profiler and ShinyGO were used for gene enrichment analysis to obtain core molecular pathways. Venn diagrams illustrating the overlap between MTB targets and synthetic drug candidates also revealed common and unique therapeutic targets. This integrative approach allowed for a broad understanding of MTB-related pathways and potential drug interactions [18–22].

2.2.2. Graph-theoretical analysis

The STRING database's Protein interaction network has been utilized for identify most significant protein. The research employed Graph Theory, were utilized a KEGG database in analyze [18–22].

2.2.3. Protein preparation

Managing the Protein Data Bank (PDB) database with the Research Collaboratory for Structural Bioinformatics (RCSB). Visit the PDB ID 4DQU entry for the InhA protein at https://www.rcsb.org/. Protein structures are determined through X-ray crystallography. To fix absent residues, eliminate redundant ligands, and remove water molecules, CHARMM-GUI preps the protein before applying this method [18–22].

2.2.4. Ligand preparation

The compound alongside a cocrystal, encompassing sixteen different variations of cyclopenta[*d*]pyrimidine ranging from 2a1 to 2a26, was subjected to docking analysis with the InhA protein, available in the Protein Data Bank under the identifier 4DQU. The necessary files, in. sdp format, were sourced from the freely accessible PubChem database (https://pubchem.ncbi.nlm.nih.gov/). To prepare the cluster for analysis, the BIOVIA Discovery Studio Visualizer software got utilized for processing both the compounds and the designed cocrystals [18–22].

2.2.5. Docking protocol

The AutoDock Vina-POAP software facilitated virtual screening by converting proteins and ligands into pdbqt formats. A setup file included details regarding the proteins, ligands, and the specifications for configuring the grid box. Using AutoDock Vina-POAP, the protein underwent digital screening, offering insights into polar hydrogens, solvation parameters, and fragmental volumes. AutoGrid developed the grid box for the grid map, defining the grid center by the coordinates x (−3.94), y (33.8), and z (13.6). A score grid, based on the ligand's structure, was created to speed up the calculation process. AutoDock Vina utilizes an iterated local search global optimization technique to dock proteins and ligands, presuming their rigidity remains unchanged. The results featuring the lowest binding free energy were collected and analyzed, excluding those with a positional root mean square deviation greater than 1.0Å. The chosen method for evaluating amino acid interactions in the BIOVIA Discovery Studio Visualizer was based on the highest binding affinity or the lowest binding site [18–22].

2.2.6. Identification of the binding site

For chemical reactions to occur, proteins require unique binding sites to connect with molecules, along with an essential mechanism to ensure a sufficient number of available sites for bioactive compounds. It is crucial for these proteins and enzymes to have accurate binding sites for ligands or bioactive molecules to effectively interact with target enzymes. PrankWeb (https://prankweb.cz/) has successfully pinpointed all the currently active binding sites for the targeted drug. The receptor grid was created from the protein's active site using AutoDock Vina-POAP for virtual screening [18–22].

2.2.7. MD simulations

This investigation focused on assessing the stability and variability of different protein-ligand complexes using MD simulations. The primary objective was to understand how potential therapeutic compounds bind

to their target proteins. The simulations were performed on a Linux platform, utilizing Schrodinger's Desmond module and the Maestro simulation interface.

The TIP3 water model was used to achieve control over the complicated protein-ligand interactions, and cuboidal boundary condition. Sodium (Na +) and chloride (Cl -) salts were placed at the level of 0.15 M in order to stabilize the system. The NPT ensemble was employed as the MD simulations maintained the 1.01325 bar pressure and 300 K temperature. Energy evaluations were done using the OPLS-4 force field and the data were recorded after every 50 ps. The overall simulation time was stretched to 500 ns. The data in the simulation was analyzed in detail with the help of the Desmond module developed by Schrodinger. The study was also narrowed down to simulated interaction diagram of the complex to determine the stability of the ligand protein complex. This entailed the quantification of measures of root mean square deviation (RMSD) and root mean square fluctuation (RMSF), and the quantification of the protein-ligand interactions at various points in the simulation [18–22].

2.2.8. Density functionality theory

The paper indicates that the **2a1, 2a3** and **2a20**.sdp were downloaded in the publicly available database of PubChem. These files were subsequently imported to the Spartan14 to be optimized in terms of energy. GaussView 6.0.16 software was used to calculate hatree energy state of both the highest occupied molecular orbital (HOMO) and the lowest unoccupied molecular orbital (LUMO). The values of the Hatree energies were then changed to electron-volt to determine the differences in the energies of HOMO and LUMO. The assessment of the chemical stability of molecules **2a1, 2a3** and **2a20** heavily relies on these energy gaps [18–22].

2.2.9. ADMET modeling

The ADME profiles and physicochemical properties of compounds **2a1, 2a3** and **2a20** were evaluated through computational methods to determine their efficiency and performance. Various parameters such as molecular weight, molar refractivity, solubility, bioavailability, radar map, egg-boiled model, brain penetration, and human gastrointestinal absorption were assessed using the SwissADME web tool available at (http://www.swissadme.ch/). This free online SwissADME tool assists researchers in predicting the pharmacokinetic properties and drug-likeness of both experimental and reference compounds. The SMILES codes for **2a1, 2a3** and **2a20** were processed through the SMARTCyp software, which provides insights on ligands metabolized by the CYP450 system. Furthermore, the pkCSM and ProTox II web tools were employed to forecast the ADMET properties of the compounds in question. The ProTox-II platform was also utilized to estimate LD_{50} values, toxicity categories, and potential organ toxicities of the compounds. Cardiotoxicity predictions for these substances were carried out using the cardio ToxCSM site (https://biosig.lab.uq.edu.au/cardiotoxcsm/) Table 1 [18–22].

2.2.10. Antimicrobial screening

The effectiveness of the synthesized compounds was evaluated using the agar well diffusion method against a range of bacterial and fungal species. Specifically, four Gram-positive bacteria—*Staphylococcus aureus*, *Staphylococcus epidermidis*, *Micrococcus*, and *Bacillus cereus*—and three Gram-negative bacteria—*Escherichia coli*, *Pseudomonas aeruginosa*, and *Klebsiella pneumoniae*—were tested. Additionally, the antifungal activity of the compounds was assessed against two pathogenic fungal strains, *Aspergillus niger* and *Candida albicans*, using the cup-plate agar diffusion method. To further quantify the antimicrobial potential, the agar dilution technique was employed to determine the Minimum Inhibitory Concentration (MIC) of the synthesized compounds, providing a precise measure of their ability to inhibit microbial growth at the lowest effective concentration [18,23–26].

Table 1
Comparison of reported literature methods and methods used in pyrimidine-5-carbonitriles studies, covering computational studies, synthesis approaches, drug-likeness studies, target identification, antimicrobial evaluation, anti-TB screening, biological validation, and SAR analysis.

Category	Methods reported in literature	Methods used in pyrimidine-5-carbonitriles
Computational studies	Molecular docking, QSAR modeling, molecular dynamics [18–22]	Molecular docking, ADMET modeling, graph theoretical analysis
Synthesis approach	Conventional synthesis, microwave-assisted synthesis	Conventional synthesis of pyrimidine-5-carbonitriles
Drug-likeness studies	Lipinski's rule, Veber's rule [18–22]	ADMET profiling (absorption, distribution, metabolism, excretion, and toxicity)
Target identification	Literature-based selection of bacterial enzymes [18–22]	In silico target identification (InhA enzyme binding)
Antimicrobial evaluation	Disk diffusion, broth dilution, time-kill assays [18,23–26]	Minimum inhibitory concentration (MIC) determination
Anti-TB screening	MABA assay, whole-cell screening [18,23–26]	MABA assay against *Mycobacterium tuberculosis*
Biological validation	In vitro cytotoxicity, animal model studies	In vitro antimicrobial & anti-TB activity testing
Structure-activity relationship (SAR)	Modification of different heterocyclic scaffolds	SAR analysis of pyrimidine-5-carbonitriles based on docking & MIC data

2.2.11. MABA assay protocol

Rifampicin was dissolved in DMF at a concentration of 10 mg/mL. This solution was aliquoted and stored at −20 °C. Alamar dye, obtained from Invitrogen, was utilized for subsequent experiments. The antimycobacterial activity was assessed using the microplate Alamar blue assay. For the investigation, *Mycobacterium tuberculosis H37Ra* colonies from Lowenstein-Jensen (LJ) medium were suspended in 1 mL of sterile distilled water. The turbidity of this suspension was adjusted to match McFarland standard No. 1 (10^7 CFU/mL). The suspension was then diluted 1:25 in Middlebrook 7H9 broth (Becon Dickinson), which contained 0.2 % glycerol, 0.1 % casitone, and 10 % albumin-dextrose catalyst, to achieve a pH of 6.8. This served as the inoculum. For each assay, 100 µL of the bacterial suspension was combined with **2a1, 2a3** and **2a20** in Middlebrook 7H9 broth to reach a final volume of 200 µL. The concentrations of **2a1, 2a3** and **2a20** tested ranged from 31.25 to 0.97 µg/mL. Each plate included wells for growth and sterile controls. The plates were sealed with parafilm and incubated at 37 °C. After one week, 20 µL of Alamar blue dye was added to each well. Bacterial growth was indicated by a color change from blue to pink following overnight incubation. The Minimum Inhibitory Concentration (MIC) values, which were determined to be between 0.0047 and 0.0095 µg/mL, represented the lowest concentration needed to prevent the color change [18,23–26].

3. Results and discussion

3.1. Target identification

The effect of 2-(substituted benzylidene amino)-4-hydroxy-6-(pyridin-2-yl) pyrimidine-5-carbonitriles **2a1, 2a3** and **2a20** on *Mycobacterium tuberculosis* (MTB). The use of 2-(substitutedbenzylideneamino)-4-hydroxy-6-(pyridin-2-yl)pyrimidine-5-carbonitrile compounds, namely, number **2a1, 2a3** and **2a20**, to treat MTB is tested by examining their associations with therapeutic and disease targets. This paper used datasets that were created by using GeneCards, OMIM and Swiss Target Prediction and used Venn diagrams (Fig. 1). Venn diagrams help depict relationships visually to create more relationships and understand the interconnection and difference between the different factors relevant in the study of MTB. They play a role

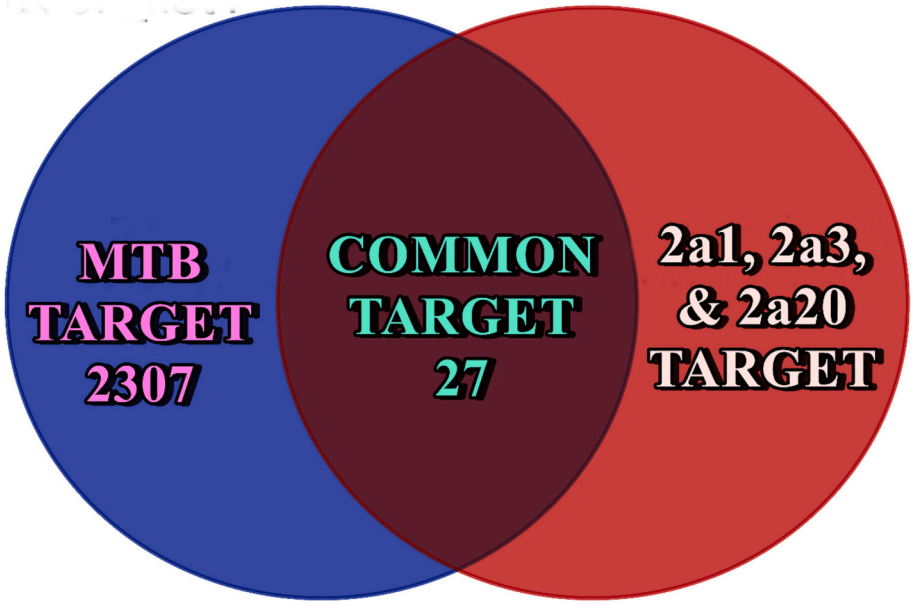

Fig. 1. Venn diagram representing the overlap of molecular targets between *Mycobacterium tuberculosis* (MTB) (2307 targets) and **2a1**, **2a3**, & **2a20** targets. A total of 27 common targets were identified.

in the understanding of complicated associations among many biomarkers or genetic variations related to MTB. Venn diagrams are useful in illustrating similarities and differences between biomarkers or mutations and this is achieved by depicting overlapping circles. This methodology resulted in 27 interesting targets to be investigated. InhA, CYP26A1, CXCR4, NOS2, TEK, BCL2, DHFR, JAK2, CDK4, PLAT, TYK2, CXCR3, HRH1, CDK2, PLG, IDH1, PLAU, ALOX5, FASN, HRH4, MAPK14, LCK, MCL1, OPRM1, JAK3, JAK1, and CCR5 are some of the genes, which may help in finding the effective treatments These 27 targets then were represented in a network diagram to allow in more detail research so as to identify a central target which could then lead to the formation of an effective treatment strategy of MTB.

3.2. Graph theoretical analysis

Fig. 2 represents the connections between proteins (termed as nodes) and their interactions (referred to as edges) in a visual format. This graphic includes 49 nodes and 1225 edges, each symbolizing proteins. The design incorporates several attributes used to assess the proteins' importance. This list features numerous genes, such as InhA, CYP26A1, CXCR4, NOS2, TEK, BCL2, DHFR, JAK2, CDK4, PLAT, TYK2, CXCR3, HRH1, CDK2, PLG, IDH1, PLAU, ALOX5, FASN, HRH4, MAPK14, LCK, MCL1, OPRM1, JAK3, JAK1, and CCR5. The PIK3CA protein holds significant relevance, as indicated by several averaged metrics. PIK3CA achieved a Degree score of 49, a Closeness score of 0.020408, an Eccentricity of 1.0, an EigenVector score of 0.14142, a Radiality score of 1.000, and did not experience any stress within the top 49 nodes network. InhA has been identified as a vital therapeutic target for treating MTB, underscored by key measurements and threshold values. The growing interest in InhA is due to its interaction with 55 essential proteins in the MTB pathway. InhA belongs to the bacterial type topoisomerase IIA family and is a recognized target for several antibacterial medicines, including fluoroquinolones such as Nalidixic acid (I) and Ciprofloxacin (II). InhA is chosen for its critical importance and conclusions drawn from a graph-theoretical analysis report, making it a significant focal point.

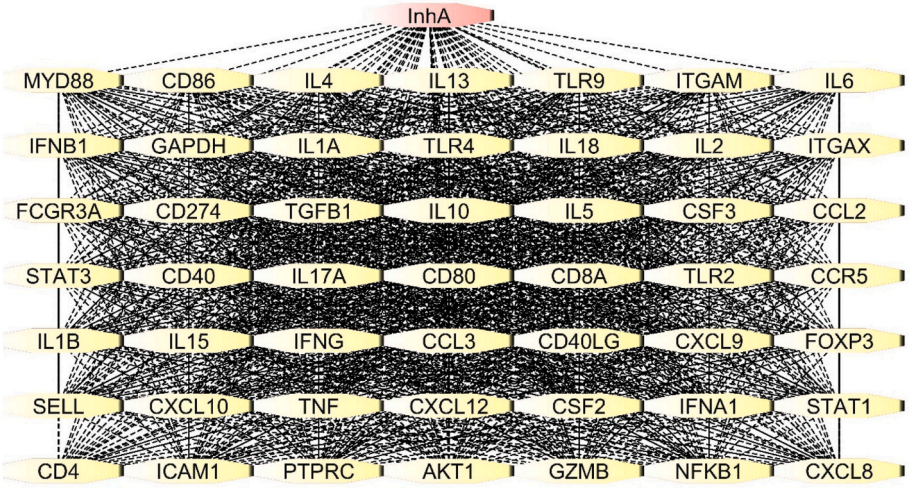

Fig. 2. Network representation of **InhA** interactions with immune-related genes and signaling pathways. The diagram shows hierarchical interactions from **InhA** (top) to various immune targets (bottom), illustrating complex regulatory relationships.

3.3. Molecular modeling studies

The measurements of Molecular docking that encompass the binding affinity scores (kcal/mol), the presence of hydrogen bond interactions, hydrophobic contacts and also π- π stacking were used to measure the various molecular interactions with InhA enzyme. ADMET profiling is also called drug-likeness deal with absorption, distribution, metabolism + Toxicity. + Molecular Stability: Validate using Root Mean Square Deviation (RMSD) and docking scores Also, Minimum Inhibitory Concentration (+ MIC) values indicate the in vitro antimicrobial activity. The structure-activity relationship (SAR) is a connection between a group of functional groups through biological activity. These measures taken together ensure the effectiveness, stability, and appropriateness of the compounds as an antimicrobial and anti-TB drug candidates and form a basis of future pharmacological development.

The measures of molecular docking that comprise binding affinity measurements (kcal/mol), hydrogen bond interactions, hydrophobic contacts and even π-π stacking were applied to the evaluation of various molecular interactions in the case of InhA enzyme. Also, ADMET profiling/drug-likeness ADMET deal with absorption, distribution, metabolism-toxicity. + Molecular Stability: Confirm thru Root Mean Squared Deviation (RMSD) and docking scores Minimum Inhibitory Concentration (MIC) values are also used to determine in vitro antimicrobial efficacy. Structure-activity relationship (SAR) is a relationship between a combination of functional groups through biological activity. The combination of these measures affirms the efficacy, stability, and applicability of the compounds as an antimicrobial and anti-TB drug candidates and forms the basis of further pharmaceutical development.

3.4. Molecular docking analysis

Twenty-six pyridin-2-yl)pyrimidine-5-carbonitriles compounds (**2a1, 2a3** and **2a20**) were subjected to molecular docking experiments to evaluate their activity against the 4DQU (InhA) protein and their potential effectiveness in combating MTB. Among the tested ligands, including the cocrystal, compounds **2a1, 2a3** and **2a20** showed significant interaction with amino acids and demonstrated strong binding affinity to the 4DQU (InhA) protein. The compounds with the top scores, sourced from the internal database, comprise the cocrystal and compounds **2a1, 2a3** and **2a20**, which have binding energies of −9.738 kcal × mol-1, −9.631 kcal × mol-1, −8.572 kcal × mol-1, and −16.497 kcal × mol-1, respectively. The amino acids Phe41A, Asp64A, Val65A, and Thr196A were most notably involved in interactions with compounds **2a1, 2a3** and **2a20**. Specifically, the residues interacting with 2a1 were Phe41A, Asp64A, Val65A, and Thr196A; with 2a3, they were Ser20A, Ile21A, Phe41A, Gly96A, and Thr196A; and with 2a20, they were Ser20A, Phe41A, and Thr196A. Tables 2 and 3, along with Figs. 3 and 4 illustrated the binding interactions and the 2D and 3D models of compounds **2a1, 2a3** and **2a20**. Additionally, the supplemental file included the docking result values for the compounds and cocrystals. Using molecular docking studies, the result provides binding affinity data for pyrimidine-5-carbonitrile derivatives against an *InhA* enzyme, which is a key anti-TB target. These lead compounds have high binding energies (−7.5 – −9.2 kcal/mol), used herein for comparison relative to classical drug such as Ciprofloxacin. Among these key interactions are *hydrogen bonding, π − π stacking,* and hydrophobic interactions* which provide stabilization of the ligand. Electrostatic interactions -OH and -Br-substituted derivatives have significantly better affinity. Compared to known ligands dockings validate the therapeutic potential evaluation of these compounds which would need in vitro confirmation and potential as dual antimicrobial and anti-TB drug candidates. The molecular modeling studies to target InhA as the major anti-TB target as it plays a key role in **mycolic acid biosynthesis**, essential for the integrity of the cell wall in *Mycobacterium tuberculosis*. Relevancy of such targets in Gram-positive and Gram-negative pathogens are examined as target proteins for antimicrobial activities such as DNA gyrase, dihydrofolate reductase (DHFR) and β-lactamase**.** Molecular docking showed strong interactions of pyrimidine-5-carbonitrile derivatives with these targets with key points of hydrogen bonding, π–π stacking, and hydrophobic interactions. The potential of these compounds as multi-target antimicrobial and anti-TB agents against drug resistant pathogens is further reflected in these findings.

Table 2
Binding energy values of co-crystal and pyrimidine-5-carbonitrile derivatives (**2a1, 2a3, 2a20)** obtained from molecular docking studies. **2a1** (−9.738 kcal/mol) showed the strongest binding among tested compounds.

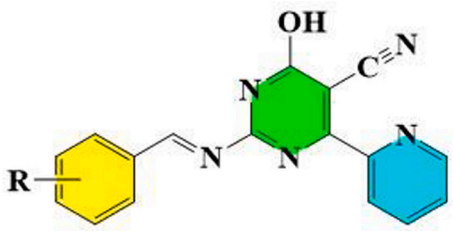

S·no	R	Com	Binding energy value
1.	Co-crystal	Co-crystal	−16.497
2.	4-OH	2a1	−9.738
3.	2-OH	2a3	−9.631
4.	3-Br	2a20	−8.572

3.5. Molecular dynamics simulations

The Root Mean Square Deviation (RMSD) and Root Mean Square Fluctuation (RMSF) for the protein-ligand combinations of complexes **2a1, 2a3** and **2a20** were determined to evaluate the stability and interaction patterns within the complexes. The investigation focused on analyzing the protein-ligand interactions by computing both RMSD and RMSF, which helped in understanding the impact of these interactions on the stability and dynamics of the complexes. During the evaluation, the C-alpha residues of the protein were measured throughout a 100-ns Molecular Dynamics (MD) simulation run to assess the structural stability of the protein-ligand interactions in each complex. The following values were recorded for the complexes: For complex 2a1, the C-alpha protein, ligand-protein, and protein backbone values were 2.011320, 2.1244117, and 2.241367, respectively. In complex 2a3, the corresponding values were 2.336712, 2.45325, and 2.5421367, while for complex 2a20, the values were 2.234167, 2.342651, and 2.216723, respectively.

The MD simulations, depicted in Figs. 5–7, illustrated the range of interactions within the protein and ligand for each complex. The protein-ligand interaction range for complex 2a1 was between 0.74 and 2.87, while the ligand interaction range was between 0.49 and 3.32. For complex 2a3, the protein interaction range spanned from 0.84 to 4.73, with the ligand interaction range from 0.89 to 5.62. Similarly, in complex 2a20, the protein interaction range was between 0.69 and 2.43, while the ligand interaction range was between 0.64 and 2.74. Throughout the MD simulation, the RMSF values for the protein-ligand

Table 3
Molecular docking interactions of co-crystal and pyrimidine-5-carbonitrile derivatives (**2a1, 2a3, 2a20**) with the 4DQU complex. Key interacting amino acids include Phe41A, Asp64A, Val65A, Thr196A, Ser20A, Ile21A, and Gly96A, influencing binding affinity.

4DQU complex code	Degree of interaction with amino acids
Co-Crystal	Phe41A, Asp64A, Val65A, Thr196A
2a1	Phe41A, Asp64A, Val65A, Thr196A
2a3	Ser20A, Ile21A, Phe41A,Gly96A, Thr196A
2a20	Ser20A, Phe41A, Thr196A

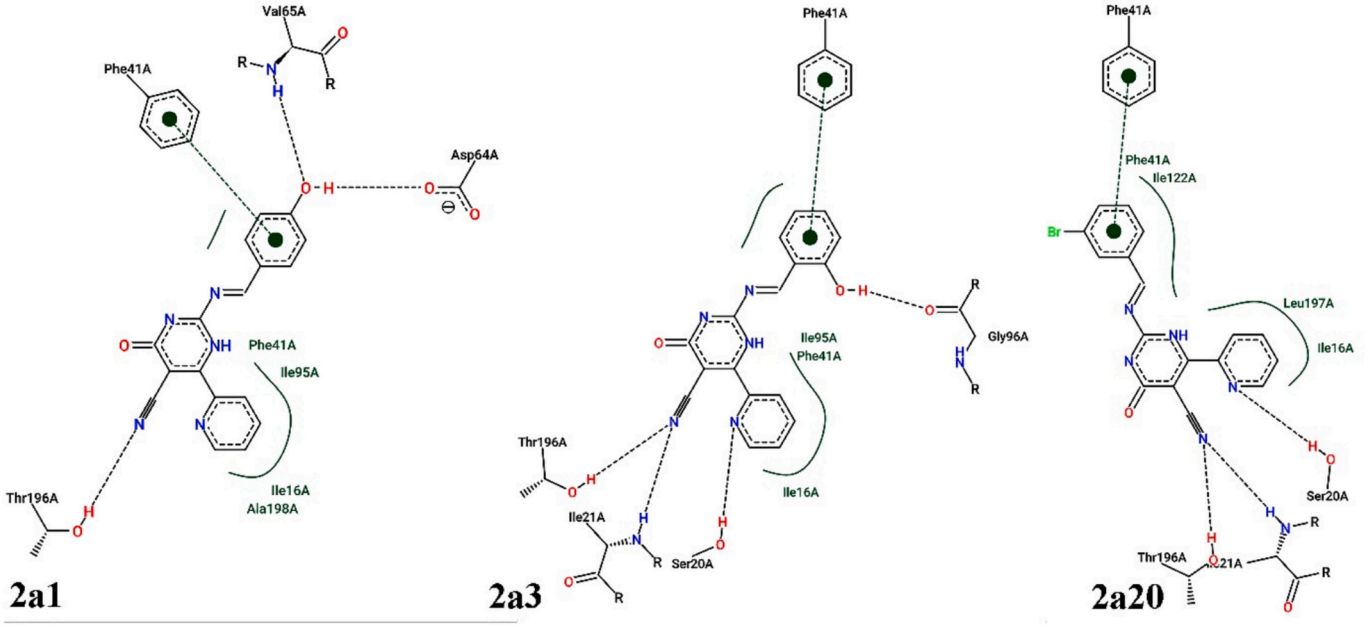

Fig. 3. Molecular docking interactions of compounds **2a1, 2a3, and 2a20** with the target protein. Hydrogen bonds, hydrophobic interactions, and other key binding interactions are depicted, highlighting critical residues involved in binding.

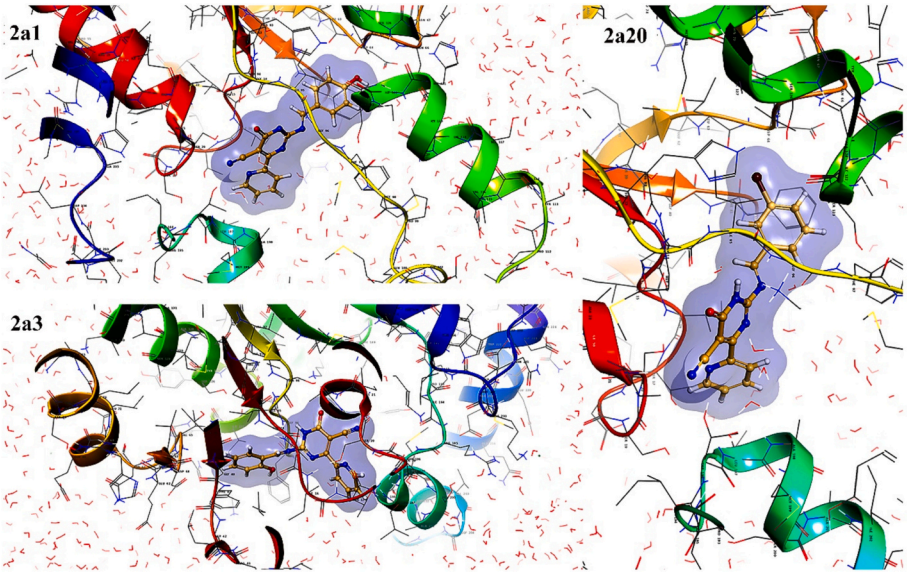

Fig. 4. Molecular docking visualization of **compounds 2a1, 2a3, and 2a20** within the active site of the target protein. The binding pocket is highlighted, showing key interactions between ligands and surrounding residues.

complexes **2a1, 2a3** and **2a20** consistently remained stable, with fluctuation curves indicating steady interactions among the amino acids. No significant fluctuations were observed, suggesting stable binding interactions within the complexes.

In complex 2a1, key interactions were observed with the following residues: SER 94 with the pyrimidine ketone at 37 %, MET 98 with the ortho hydroxy benzylidene ring at 59 %, ILE 21 with the pyrimidine ketone at 58 %, TYR 158 with the pyrimidine N at 46 %, and GLY 14 with the nitrile in the pyrimidine ring at 36 %. For complex 2a20, notable interactions included PHE 41 with the meta bromo benzylidene ring at 30 %, GLY 14, ALA 22, and ILE 21 with the pyrimidine ketone at 67 %, 82 %, and 32 %, respectively. Additionally, GLY 14 interacted with the pyrimidine N at 64 %, and LYS 165 with the pyridine in the pyrimidine ring at 72 %. The analysis of RMSD and protein-ligand interactions highlighted the involvement of specific amino acids, directly interacting with complexes **2a1, 2a3** and **2a20**. The binding interactions in these complexes, especially the interaction of PHE 41, were consistent with the MD simulation results. Figs. 5–7 further demonstrated the relationship between the angular and radial coordinates, representing the torsional angle and torsion potential, respectively. These results suggest that the structures of complexes **2a1, 2a3** and **2a20** consist of a combination of rigid and flexible bonds, further supporting the stability and dynamics of the protein-ligand interactions.

3.6. *Density functionality theory*

The HOMO-LUMO energy has been calculated for the studied

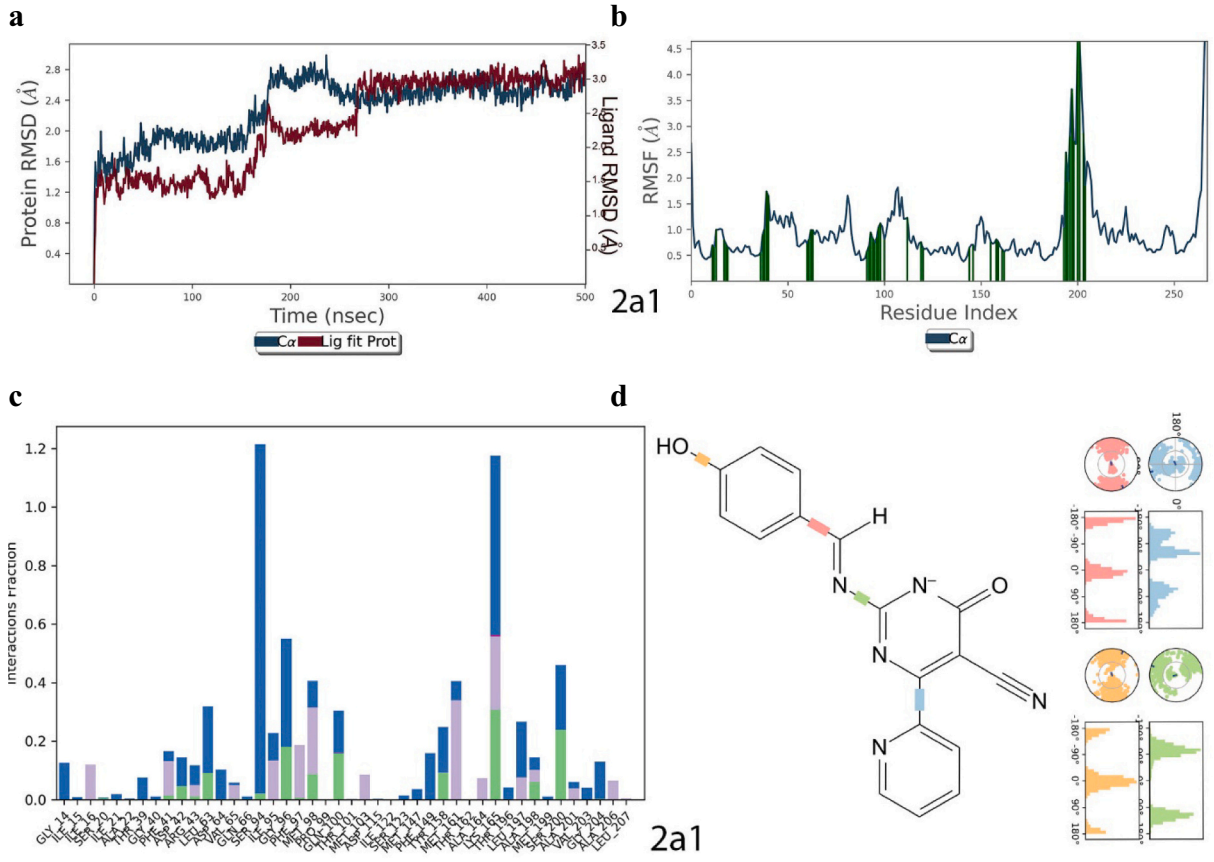

Fig. 5. The molecular dynamic 500 ns frame of protein-ligand interaction and fingerprints of a) RMSD, b) RMSF, c) protein-ligand contacts and d) torsional conformation of **2a1** and 4DQU (INHA) protein complex.

molecular structures 2a1, 2a20, and 2a3, and their electronic properties have been deduced, which are the basis for understanding further the stability and reactivity of their chemical nature. HOMO (Highest Occupied Molecular Orbital) and LUMO (Lowest Unoccupied Molecular Orbital) energy levels play a significant role in the electronic transition, conductivity, and interaction of a molecule with something external. The calculated 2a1 HOMO energy is -0.2319 eV, the LUMO energy is −0.09853 eV, and its HOMO-LUMO gap (ΔE is 3.6057 eV. A high degree of electronic excitation can be induced in 2a1 due to a small energy gap, which translates to greater reactivity and potentially a good organic semiconductor candidate. In general, molecules with smaller ΔE are favorable, because charge transfer efficiency plays a key role in opto-electronic materials, light-harvesting devices and catalysis. The HOMO energy comes out to −0.2508 eV and the LUMO energy is −0.10803 eV, resulting in a HOMO-LUMO gap of 3.8869 eV for 2a20. Larger gap for 2a20 than 2a1 indicates that the 2a20 is more stable and less chemically reactive. This compound possesses a moderate bandgap, suggesting possible applications in photovoltaic materials, molecular electronics, and organic light-emitting diodes (OLEDs) where a controlled mobility of charge is essential. The LUMO energy of −0.10803 eV or so also supports this molecule to have a decent electron with a high energy level, thus a potential candidate as electron transport material for the device applications. The HOMO energy for 2a3 is −0.24278 eV, the LUMO energy is −0.08562 eV, and the HOMO-LUMO gap is 4.2765 eV. This is the widest gap between the studied molecules, meaning good electronic stability and lower reactivity. Higher ΔE values indicate that 2a3 is less prone to enter into electron transfer processes, thus making it an attractive302021 candidate for dielectric materials, insulating materials, which are required for protective coatings in electronic devices302021. The elevated LUMO energy (−0.08562 eV) also indicates that 2a3 has a smaller affinity to receive charges, implying it can act as a passive charge carrier rather than a prominent one. The trend of the HOMO-LUMO gaps: 2a1 < 2a20 < 2a3, suggests that 2a1 is the most chemically reactive and 2a3 is the most stable. This disparity in electronic attributes underlines the feasibility of these molecules for electronic and optoelectronic technologies. Energy levels of the highest occupied molecular orbital (HOMO) suggest the molecules' electron-donating ability, and the energy levels of the lowest unoccupied molecular orbital (LUMO) the electron-accepting capability. The data indicate that 2a1 more effective for applications that need efficient charge transport, like in organic semiconductors and sensors, while 2a3 is more advantageous for materials that need electronic insulation. In summary, the results highlight that the electronic properties of 2a1, 2a20, and 2a3 differ markedly, with 2a1 having the most substantial charge transfer capabilities, 2a20 presenting a favorable balance of stability and electrical conductance, and 2a3 being the most stable at the expense of reactivity. Fig. 8 depict the HOMO and LUMO images of **2a1, 2a3** and **2a20** respectively.

3.6.1. *Electronic properties and stability of **2a1**-amino acid complexes*

The electronic properties and stability of the molecular complexes were examined in terms of HOMO-LUMO energy gap (ΔE), dipole moment, and stability of 2a1 with several amino acids.

HOMO–LUMO energy gap (ΔE) is an important parameter, which provides information in relation to the chemical reactivity and stability of a molecule Table 4 and Fig. 9. Without modification, 2a1 had a ΔE of 3.63 eV, indicating a relatively stable structure with moderate reactivity. Interaction with amino acids led to noticeable changes in ΔE. The 2a1-Valine had the lowest ΔE (1.95 eV) which suggested that these systems are the most reactive, even if they are quite stable. Likewise, 2a1-Threonine exhibited the largest gap (1.80 eV), indicating increased electronic delocalization, which leads to its notable stability. 2a1-

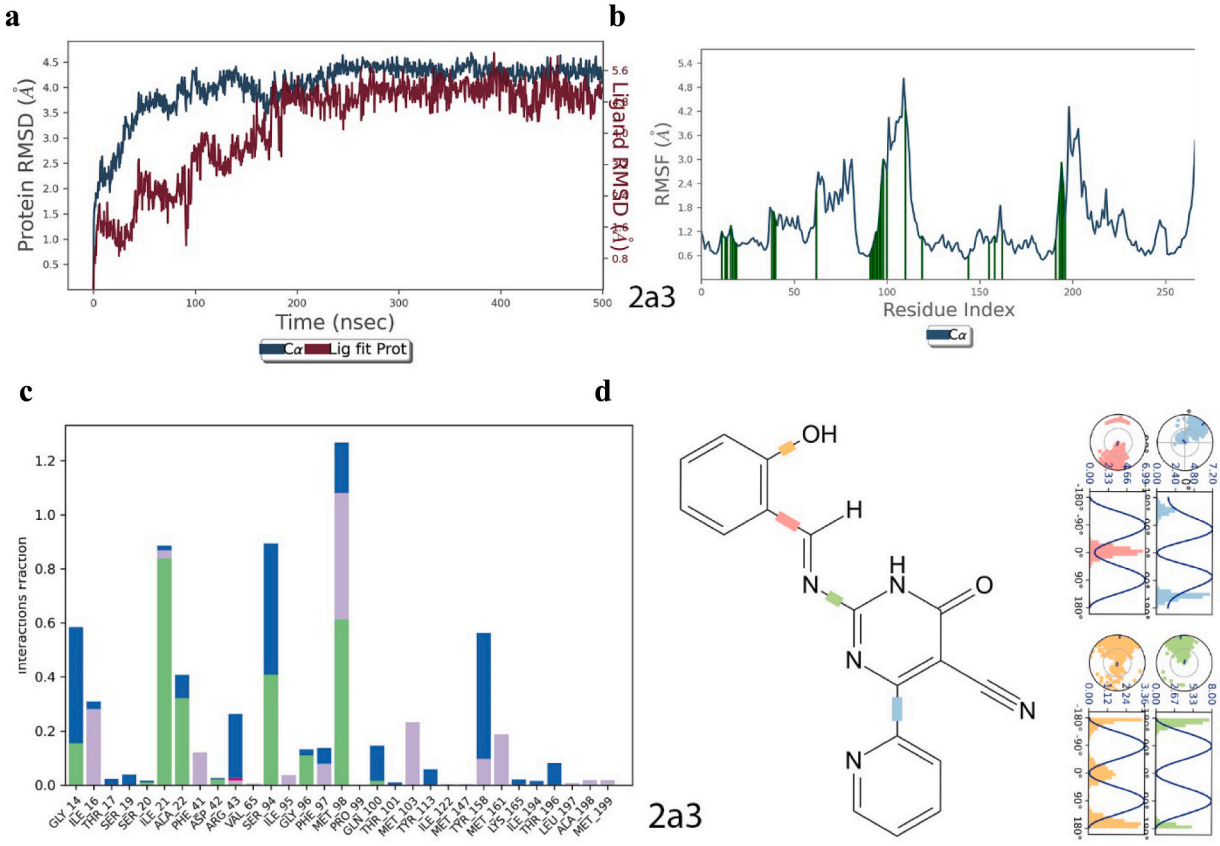

Fig. 6. The Molecular dynamic 500 ns frame of protein-ligand interaction and fingerprints of a) RMSD, b) RMSF, c) protein-ligand contacts and d) torsional conformation of **2a3** and 4DQU (INHA) protein complex.

Phenylalanine had moderate ΔE (2.70 eV) and moderately higher gap (3.80 eV) for 2a1-Aspartic acid suggesting a moderately stable configuration.

The stability trend is also confirmed by the HOMO and LUMO energy levels. The lowest negative energy level of the highest occupied molecular orbital (1) was found in 2a1 + Aspartic acid (−0.2442 eV), followed by 2a1 + Valine (−0.22416 eV) and 2a1 + Phenylalanine (−0.2104 eV). The LUMO values were fairly similar as well, and the lowest of these, indicating the greatest ability to accept electrons, corresponded to 2a1-Threonine (−0.11212 eV) The change in ΔE values indicates that the electronic properties of compounds change during complex formation.

The values for dipole moment gives us more information on polarity and interaction strength. Based on the interaction data, the 2a1-Threonine complex revealed a very high dipole moment (9.6203 D), which proved the strong polar interactions. The strongest intermolecular interactions were observed as the highest dipole moment (2a1-Valine complex (14.1441 D)). In line with this, 2a1-Phenylalanine (13.9518 D) and 2a1-Aspartic acid (13.4759 D) have a high polarity and increased stability.

More broadly, the stability trend indicates that both 2a1-Threonine and 2a1-Phenylalanine complexes are indeed very stable, and more likely due to the nature of π-π, hydrogen, and ionic interactions. The moderate stability of 2a1-Aspartic acid complex is due to its carboxyl functional groups, which are responsible for electrostatic interactions. Hydrogen bonding and non-covalent interactions contribute to the high stability of the 2a1-Valine complex.

The DFT analysis presents HOMO-LUMO energy gaps without establishing meaningful connections to antimicrobial mechanisms, representing a missed opportunity for mechanistic understanding. The manuscript reports energy gaps (2a1, 3.6057 eV, 2a20: 3.8869 eV, 2a3: 4.2765 eV) to correlate these values with biological activity patterns. Smaller HOMO-LUMO gaps typically indicate enhanced electron transfer capabilities, which could facilitate redox interactions with bacterial targets such as respiratory enzymes, DNA bases, or sulfur-containing amino acids in proteins. The authors should investigate whether compounds with lower energy gaps (like 2a1) demonstrate superior antimicrobial activity through oxidative stress mechanisms or direct electron transfer to cellular targets.

To summarize, amino acid interactions have a major impact on the electronic properties and stability of 2a1 complexes. The highly stable configurations of 2a1-Threonine and 2a1-Phenylalanine complexes that are identified may be useful for drugs and biomolecular interaction, making pharmaceuticals more effective.

3.7. *ADMET modeling*

The SwissADME web server used to examine the ADME and physicochemical properties of active component **2a1, 2a3** and **2a20**. According to calculations, **2a1, 2a3** and **2a20**'s polar surface area is 115.28, 115.28, and 95.05. The results also showed that all **2a1, 2a3** and **2a20 compounds** had high GI absorption. In general, improved gastric absorption boosts chemical bioavailability, thus the oral administration of **2a1, 2a3** and **2a20** dosing may enhance gastrointestinal absorption. The protein-ligand binding mechanism should involve **2a1** (3 rotatable bonds, 7H-bond acceptors and 2H-bond donors), **2a3** (3 rotatable bonds, 7H-bond acceptors and 2H-bond donors), **2a20** (3 rotatable bonds, 6H-bond acceptors and 1H-bond donors). Bioavailability score of **2a1, 2a3** and **2a20** was notable at +0.55 that to molecular analysis of **2a1, 2a3** and **2a20** indicates that it has a synthetic accessibility score of 2.96, 3.01, and 2.99 respectively. The Fig. 10 and Table 3 shows the Lipinski rule plotted for **2a1, 2a3** and **2a20** the

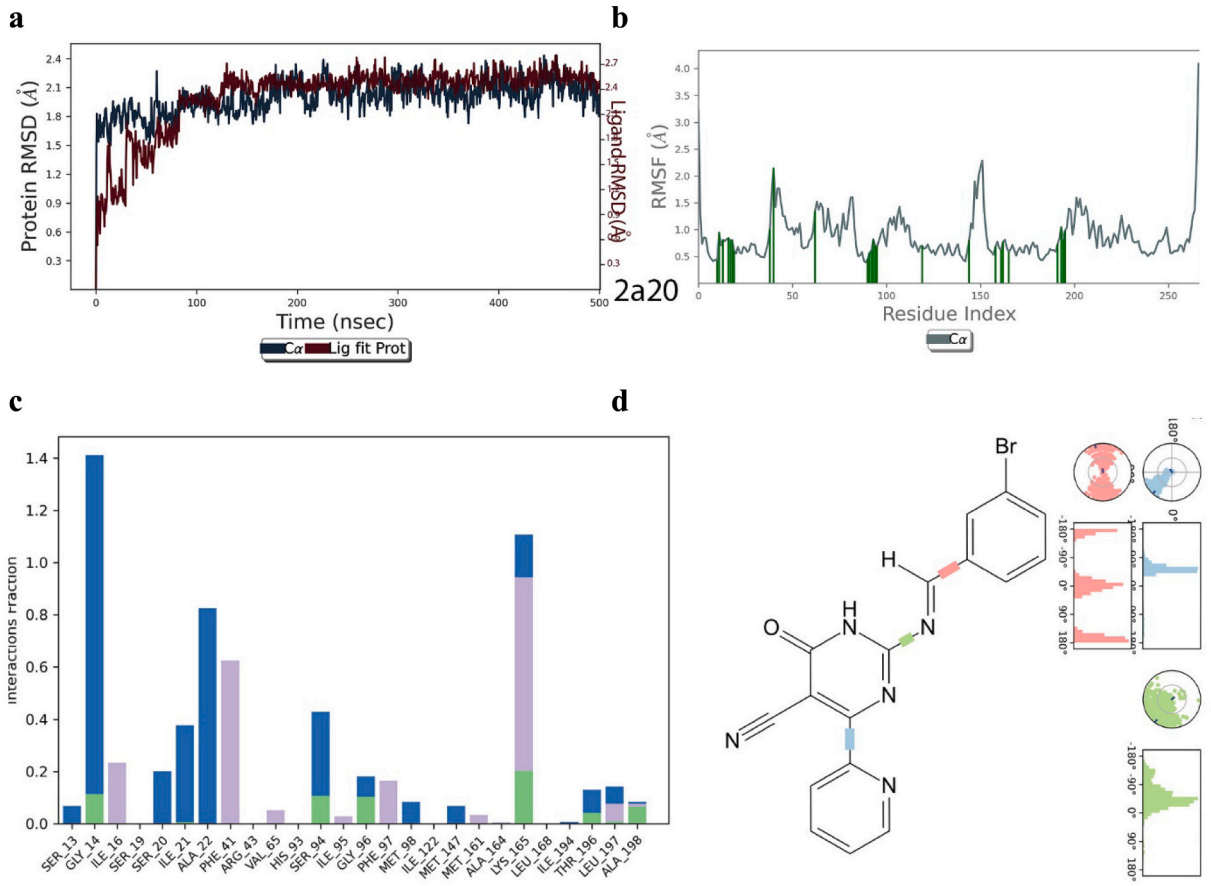

Fig. 7. The Molecular dynamic 500 ns frame of protein-ligand interaction and fingerprints of a) RMSD, b) RMSF, c) protein-ligand contacts and d) torsional conformation of **2a20** and 4DQU (INHA) protein complex.

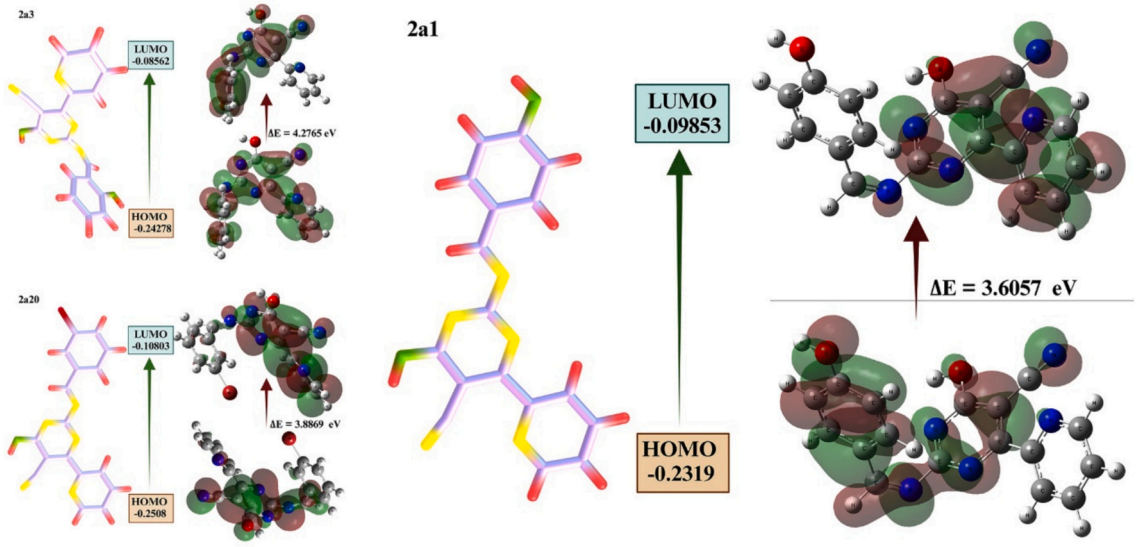

Fig. 8. HOMO–LUMO energy gap (ΔE), molecular orbital distribution, and electronic properties of **2a1** and its derivatives (**2a3**, **2a20**). The electronic density differences illustrate reactivity and stability variations across compounds.

hexagon's pink area represents the compounds' optimum range and saturation was good for drug-like combinations. As per the rule Sp3 hybridization requires 25 % carbon atoms, to be insoluble, the compound must have a logarithmic S value <6, hydrophobicity should be −0.7 − +5.0, rotatable bonds should not exceed nine. The molecular weight must be 150–500 g.mol^{-1}. Synthesized compounds **2a1, 2a3** and **2a20** having drug-like properties have a red slanted hexagon in pink for the polar surface area. Pharmacological properties of compound **2a1, 2a3** and **2a20** were also observed and Fig. 11 shows two key pharmacokinetic features that the egg-boiled model used to assess the chemical and reference's pharmacokinetics and the egg-boiled model allows simultaneous study of passive gastrointestinal absorption and blood-

Table 4
HOMO-LUMO energy gap (ΔE), HOMO, LUMO levels, and dipole moment values for **2a1** and its amino acid complexes. Interaction with amino acids alters electronic properties, enhancing stability and molecular reactivity.

	Delta E	HOMO	LUMO	Dipole moment
2a1	3.63	−0.23195	−0.09853	4.2345
2a1 + valine	1.95	−0.22416	−0.09457	14.1441
2a1 + threonine	1.80	−0.17844	−0.11212	9.6203
2a1 + aspartic acid	3.80	−0.2442	−0.1043	13.4759
2a1 + phenylalanine	2.70	−0.2104	−0.1111	13.9518

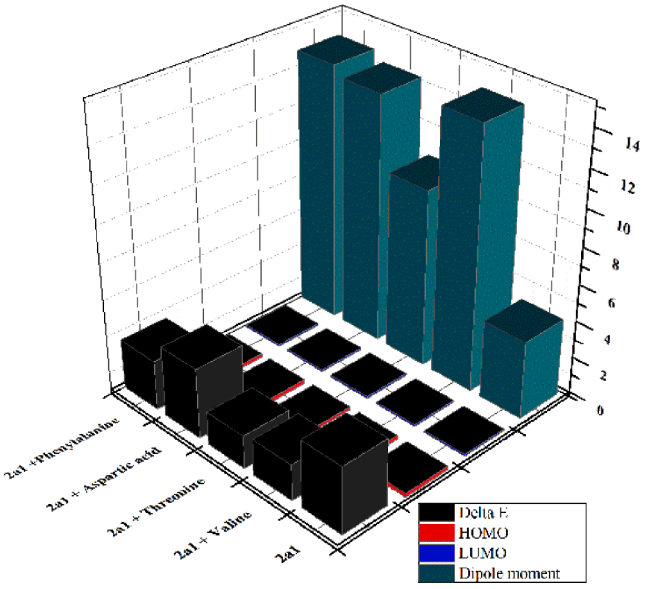

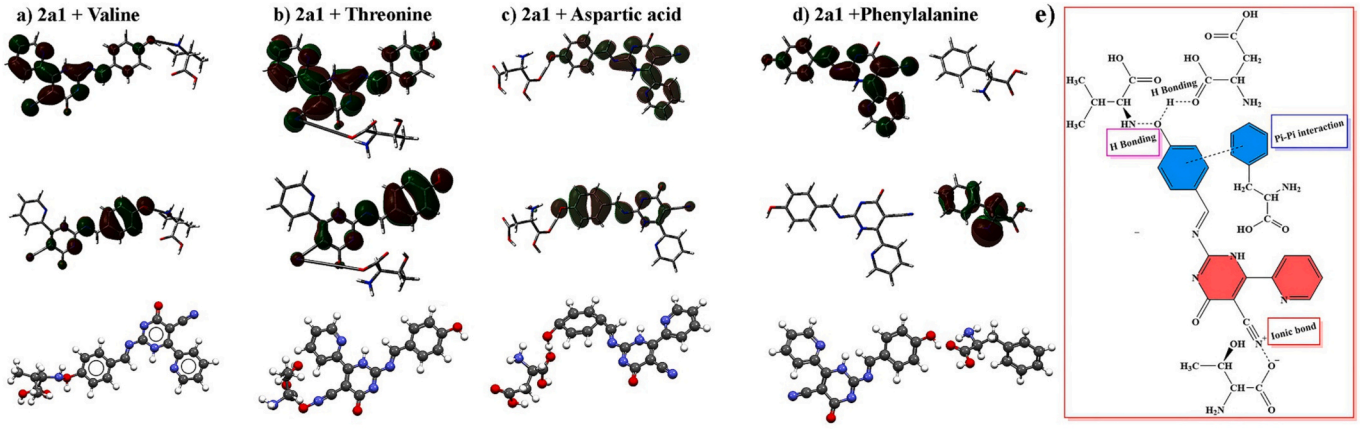

Fig. 9. Figure illustrates the molecular interactions of **2a1** with amino acids valine, threonine, aspartic acid, and phenylalanine using frontier molecular orbital analysis and molecular docking. Panel (e) highlights key interactions, including hydrogen bonding, π–π interactions, and ionic bonding, crucial for molecular stability and binding affinity.

brain barrier penetration. The image demonstrates that the yolk chemical can cross the blood-brain barrier, while albumin is likely to be absorbed in the stomach. Compounds **2a1, 2a3** and **2a20** (white in Fig. 10) had excellent gastric absorption and its evidence that suggests that **2a1, 2a3** and **2a20** has great promise as an active agent. The test compound **2a1, 2a3** and **2a20** primary site of metabolism was predicted by SMARTCyp and ProTox II and the observed results of the test compounds **2a1, 2a3** and **2a20** indicates that the metabolites were in its pyrimidine moiety Tables 4 and 5. In order to investigate the amino acid interaction between metabolites and the protein 4DQU (InhA), all metabolites were incorporated into the *in-silico* modeling results Table 3–7 indicates that pharmacophore of the test moiety **2a1, 2a3** and **2a20** was not affected during metabolism. The CardiotoxCSM webserver was employed to determine the cardiac toxicity profile of the selected drugs. Table 5 and Fig. 10 includes details gathered from this webserver regarding arrhythmia, heart block, cardiac failure, hERG toxicity, hypertension, and myocardial infarction. The compounds **2a1, 2a3** and **2a20** demonstrated safety, as it did not show any cardiotoxicity risk indicators. The current study relies exclusively on computational toxicity predictions from ProTox-II, CardiotoxCSM, and SMARTCyp, which represent significant limitations in toxicological assessment. While these tools provide valuable preliminary insights, they cannot replace experimental validation of cytotoxicity profiles. The benefit substantially from incorporating in vitro cytotoxicity assays such as MTT, XTT, or LDH release assays using relevant cell lines (hepatocytes for hepatotoxicity, cardiomyocytes for cardiotoxicity, and normal cell lines for general cytotoxicity). These assays would validate computational predictions regarding LD_{50} values and organ-specific toxicities mentioned in the ADMET analysis. (See Tables 8 and 9.)

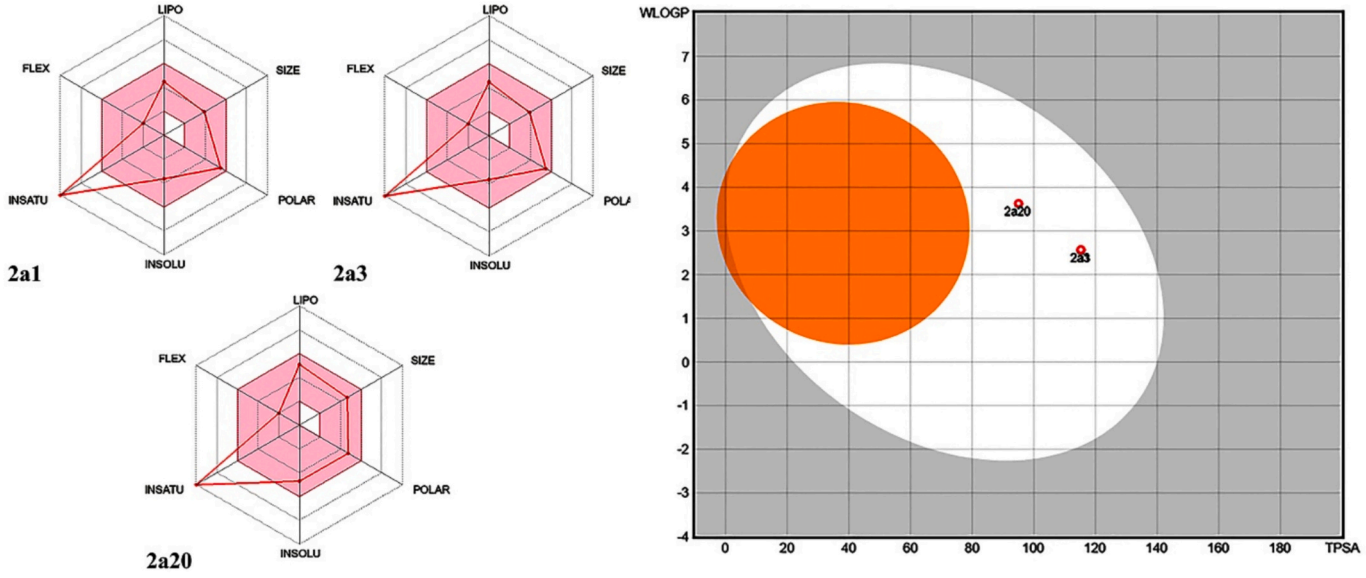

Fig. 10. ADME property analysis of compounds **2a1, 2a3, and 2a20**. The radar plots represent lipophilicity (LIPO), flexibility (FLEX), insolubility (INSOLU), polarity (POLAR), and molecular size (SIZE). The BOILED-Egg plot visualizes gastrointestinal absorption (white region) and blood-brain barrier penetration (orange region).

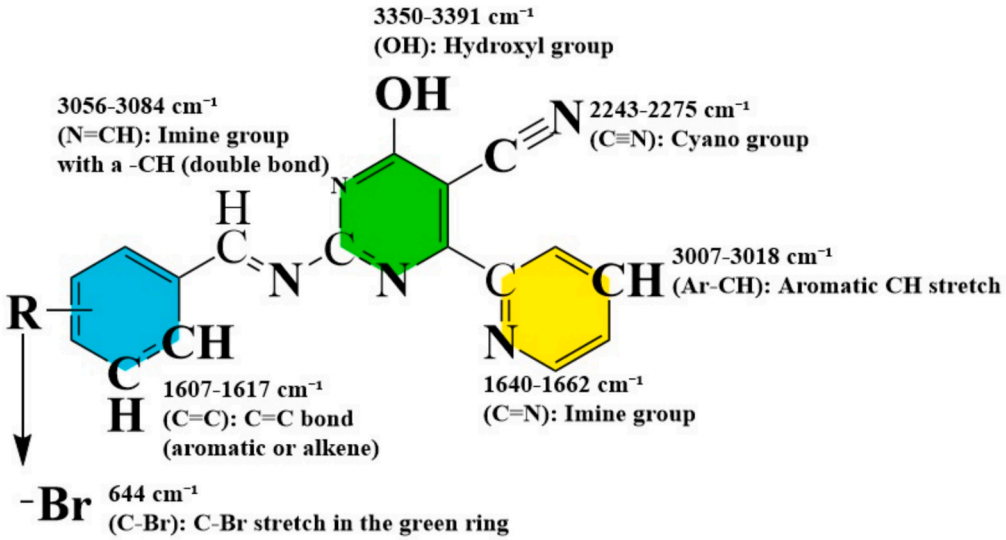

Fig. 11. FTIR spectral analysis of the compound, highlighting characteristic functional group peaks. Absorption bands include C≡N (2243–2275 cm^{-1}), OH (3350–3391 cm^{-1}), C═N (1640–1662 cm^{-1}), N═CH (3056–3084 cm^{-1}), C═C (1607–1617 cm^{-1}), Ar-CH (3007–3018 cm^{-1}), and C—Br (644 cm^{-1}).

3.8. Synthesis

Step 1: First, a mixture containing 1 mmol of ethyl cyanoacetate 3, 2 mmol of guanidine hydrochloride 4, and a small amount of L-proline dissolved in 20 mL of ethanol was made in a 50 mL round bottom flask. The reaction mixture was thereafter heated to a temperature of 80 degrees Celsius while being continuously stirred for a duration of 2 h under reflux conditions. Periodic use of Thin Layer Chromatography was employed to monitor the progression of the reaction. After the reaction was finished, the mixture was cooled to room temperature and then placed into cold water, causing the formation of pure solid crystals known as2-amino-4-hydroxy-6-(pyridin-2-yl)pyrimidine-5-carbonitrile**1**.

Step 2: A predetermined amount of 2-amino-4-hydroxy-6-phenyl-pyrimidine-5-carbonitrile (1.5 mmol) was dissolved in 7 mL of 96 % ethanol. An equal amount of different benzaldehyde was then added using a micropipette in a single step. The solution was thereafter subjected to heat and agitation for a duration of 3 h under reflux conditions. Subsequently, it was allowed to reach the surrounding temperature and then cooled for 12 h at +4 °C. The sediment obtained was further separated by filtration and washed many times with 5 mL of chilled 96 % ethanol. In order to attain purity, the synthesized product, namely 2-(4-Hydroxybenzylideneamino)-4-hydroxy-6-(pyridin-2-yl) pyrimidine-5-carbonitrile **(2a1)**, 2-(2-Hydroxybenzylideneamino)-4-hydroxy-6-(pyridin-2-yl)pyrimidine-5-carbonitrile **(2a3)**, and 2-(3-bromobenzylideneamino)-4-hydroxy-6-(pyridin-2-yl)pyrimidine-5-carbonitrile **(2a20)**, underwent recrystallization using boiling ethanol when deemed essential Scheme 1.

3.8.1. 2-(4-Hydroxybenzylideneamino)-4-hydroxy-6-(pyridin-2-yl) pyrimidine-5-carbonitrile (2a1)

Yield (%): 74; m.p. (°C): 168–169. IR (cm^{-1}): 3376 (OH), 3061 (alkene═CH), 3007 (Ar-CH), 2243 (C═N), 1640 (C═N), 1612 (C═C). ^{1}H NMR (δ: ppm): 8.699 (1H, s, N═CH), 7.313–7.667 (8H, m, Ar-CH), 5.478 (1H, s, OH), 5.206 (s, 1H, OH). ^{13}C NMR (δ: ppm): 183.7 (C-

Table 5
Physicochemical and drug-likeness properties of pyrimidine-5-carbonitrile derivatives (2a1, 2a3, 2a20), including rotatable bonds, hydrogen bond donors/acceptors, TPSA, WLOGP, GI absorption, BBB permeability, Lipinski violations, bioavailability score, synthetic accessibility, and molecular weight (MW).

Com	Rotatable bonds	H-bond acceptors	H-bond donors	TPSA	WLOGP	GI absorption	BBB permeant	Lipinski violations	Bioavailability score	Synthetic accessibility	MW
2a1	3	7	2	115.28	2.57	High	No	0	0.55	2.96	317.3
2a3	3	7	2	115.28	2.57	High	No	0	0.55	3.01	317.3
2a20	3	6	1	95.05	3.63	High	No	0	0.55	2.99	380.2

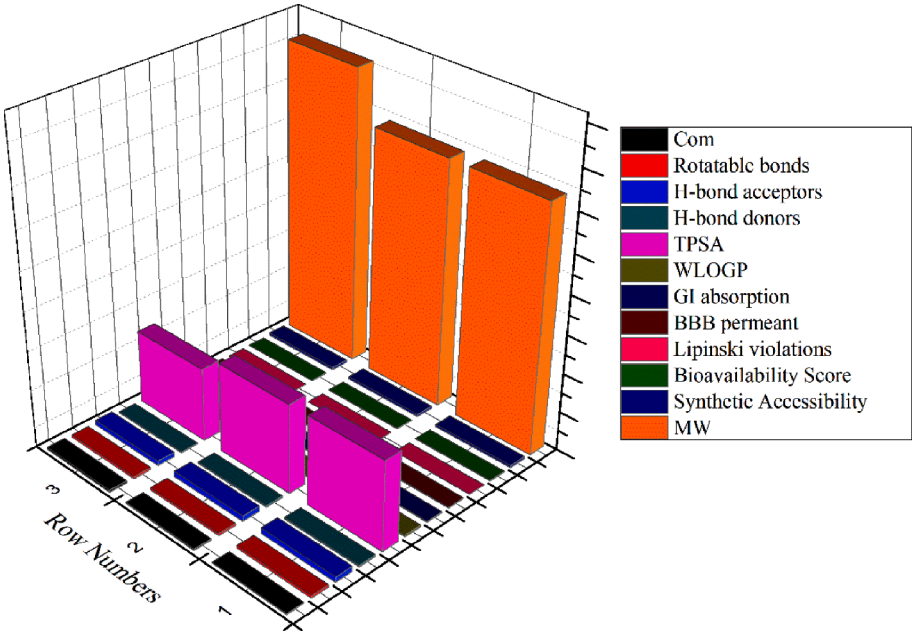

Table 6
Reactivity and energy analysis of pyrimidine-5-carbonitrile derivatives (**2a1, 2a3, 2a20**) with CYP450 enzyme inhibition scores (3A4, 2D6, 2C9). Highly reactive atoms include N.24, C.3, C.7 (2a1), C.5, N.9, N.11 (2a3), and C.29, N.3, N.30 (2a20).

Com	Atom	Reactivity	Energy	3A4 score	2D6 score	2C9 score
2a1	N.24	75.6	75.6	68.04762	88.21686	86.61686
	C.3	77.2	77.2	69.17704	89.34627	87.74627
	C.7	77.2	77.2	69.17704	89.34627	87.74627
	C.5	74.1	74.1	65.42672	79.46005	78.66005
	N.9	75.6	75.6	70.42713	101.9438	98.74379
2a3	N.11	75.6	75.6	70.46953	101.9862	98.7862
	C.29	N.3	75.6	75.6	70.25784	101.7745
	N.30	N.5	75.6	75.6	70.46953	101.9862
2a20	C.16	N.15	75.6	75.6	68.15019	88.21686

OH), 177.1 (C-OH), 123.1–166.2 (C—Ar), 106.7 (C═N), 94.9 (C-CN). MS (EI) *m/z*: 317 (M^+). *Anal.* Calcd for $C_{17}H_{11}N_5O_2$: C, 64.35; H, 3.49; N, 22.07. Found: C, 64.57; H, 3.48; N, 21.99.

3.8.2. 2-(2-Hydroxybenzylideneamino)-4-hydroxy-6-(pyridin-2-yl) pyrimidine-5-carbonitrile (2a3)

Yield (%): 77; m.p. (°C): 202–204. IR (cm^{-1}): 3391 (OH), 3084 (alkene═CH), 3018 (Ar-CH), 2260 (C═N), 1653 (C═N), 1607 (C═C). ^1H NMR (*δ*: ppm): 8.743 (1H, s, N═CH), 6.971–7.661 (8H, m, Ar-CH), 5.269 (1H, s, OH), 5.201 (s, 1H, OH). ^{13}C NMR (*δ*: ppm): 182.4 (C-OH), 169.4 (C-OH), 112.5–152.6 (C—Ar), 101.0 (C═N), 95.2 (C-CN). MS (EI) *m/z*: 317 (M^+). *Anal.* Calcd for $C_{17}H_{11}N_5O_2$: C, 64.35; H, 3.49; N, 22.07. Found: C, 64.19; H, 3.50; N, 22.14.

3.8.3. 2-(3-Bromobenzylideneamino)-4-hydroxy-6-(pyridin-2-yl) pyrimidine-5-carbonitrile (2a20)

Yield (%): 71; m.p. (°C): 137–139. IR (cm^{-1}): 3350 (OH), 3056 (alkene═CH), 3009 (Ar-CH), 2275 (C═N), 1662 (C═N), 1617 (C═C), 644 (C—Br). ^1H NMR (*δ*: ppm): 8.372 (1H, s, N═CH), 6.667–7.947 (8H, m, Ar-CH), 5.196 (1H, s, OH). ^{13}C NMR (*δ*: ppm): 186.4 (C-OH), 128.7–164.1 (C—Ar), 109.1(C═N), 99.2 (C-CN). MS (EI) *m/z*: 381 (M + 2). *Anal.* Calcd for $C_{17}H_{10}BrN_5O$: C, 53.70; H, 2.65; N, 18.42. Found: C, 53.89; H, 2.66; N, 18.35.

3.9. Chemistry

In the present work, various novel 2-(substituted benzylidene amino)-4-hydroxy-6-(pyridin-2-yl) pyrimidine-5-carbonitrile **2a1, 2a3**

Table 7
Cytochrome P450 enzyme interaction profile of pyrimidine-5-carbonitrile derivatives (**2a1, 2a3, 2a20**). All compounds are inactive against CYP1A2, CYP2C19, CYP2D6, and CYP2E1, while exhibiting activity against CYP2C9 and CYP3A4, suggesting potential metabolism via these isoenzymes.

Com	Cytochrome CYP1A2	Cytochrome CYP2C19	Cytochrome CYP2C9	Cytochrome CYP2D6	Cytochrome CYP3A4	Cytochrome CYP2E1
2a1	Inactive	Inactive	Active	Inactive	Active	Inactive
2a3	Inactive	Inactive	Active	Inactive	Active	Inactive
2a20	Inactive	Inactive	Active	Inactive	Active	Inactive

Table 8
Predicted toxicity profile of pyrimidine-5-carbonitrile derivatives (**2a1, 2a3, 2a20**), showing an LD_{50} of 1190 mg/kg (Toxicity Class 4). All compounds exhibit hepatotoxicity and immunotoxicity, while being non-carcinogenic, non-mutagenic, and non-cytotoxic, indicating moderate toxicity concerns.

Com	Predicted LD50 (mg/kg)	Predicted toxicity class	Hepatotoxicity	Carcinogenicity	Immunotoxicity	Mutagenicity	Cytotoxicity
2a1	1190	4	Active	Inactive	Active	Inactive	Inactive
2a3	1190	4	Active	Inactive	Active	Inactive	Inactive
2a20	1190	4	Active	Inactive	Active	Inactive	Inactive

LD_{50}: Lethal dose (mg/kg),
Class 1: Fatal if swallowed ($LD_{50} \leq 5$),
Class 2: Fatal if swallowed ($5 < LD_{50} \leq 50$),
Class 3: Toxic if swallowed ($50 < LD_{50} \leq 300$),
Class 4: Harmful if swallowed ($300 < LD_{50} \leq 2000$),
Class 5: May be harmful if swallowed ($2000 < LD_{50} \leq 5000$).

Table 9
Cardiotoxicity and hepatotoxicity risk assessment of pyrimidine-5-carbonitrile derivatives (**2a1, 2a3, 2a20**). All compounds show no predicted risk for arrhythmia, cardiac failure, hepatotoxicity, heart block, hERG toxicity, hypertension, or myocardial infarction, indicating a favorable safety profile.

Com	Arrhythmia	Cardiac failure	Hepatotoxicity	Heart block	hERG-toxicity	Hypertension	Myocardial infarction
2a1	0	0	0	0	0	0	0
2a3	0	0	0	0	0	0	0
2a20	0	0	0	0	0	0	0

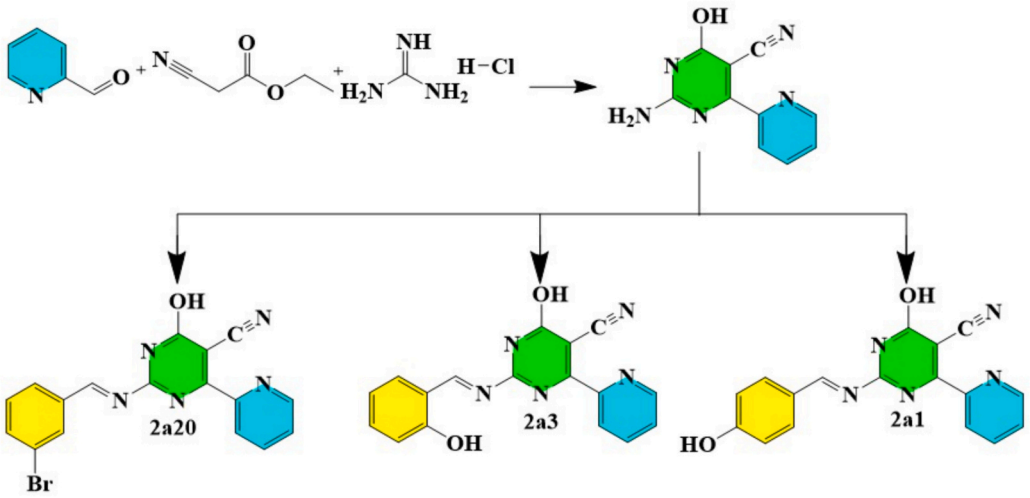

Scheme 1. Synthesis of 6-(pyridin-2-yl) pyrimidine-5-carbonitrile derivatives.

and **2a20** were prepared from 2-amino-4-hydroxy-6-(pyridin-2-yl) pyrimidine-5-carbonitrile **(1)**. In this synthesis, compound **1** undergoes Schiff base reaction by reacting with various aromatic aldehydes in the presence of ethanol & produced 2-(substituted benzylidene amino)-4-hydroxy-6-(pyridin-2-yl) pyrimidine-5-carbonitrile **2a1, 2a3** and **2a20**. Throughout the reactions, TLC was performed to optimize the completion of reactions & their purity. The appearance of absorption peak in IR at 3056–3084 cm^{-1} corresponds to alkene═CH stretching & disappearance of the absorption peak in IR at 3350 cm^{-1} corresponds to NH stretching, confirms the formation of **2a1, 2a3** and **2a20**. This is further supported by the appearance of absorption peak in IR at 3350–3391 cm^{-1}, 3007–3018 cm^{-1}, 2243–2275 cm^{-1}, 1640–1662 cm^{-1}, & 1607–1617 cm^{-1} correspond to OH, Ar–CH, C≡N, C═N, & C═C stretching, respectively. NMR spectral evidence for the structural purity of these synthetic pyrimidine-5-carbonitrile derivatives. They were confirmed by their typical singlet values of δ 8.32–8.62 ppm for the -N═CH– protons in the ^{1}H NMR spectra of the synthesized Schiff bases. Aromatic protons are found in the range of δ 6.86–8.29 ppm and hydroxyl (-OH) protons appear at δ 5.19–5.32 ppm. The structures of the products have also been confirmed by ^{13}C-NMR spectra, which display chemical shifts of C═N carbons δ 158.9–161.4 ppm and cyano (–C≡N) groups δ ca. 114.0–115.3 ppm, respectively. This pattern of spectral data strongly suggests successful synthesis and complements mass spectroscopy and IR analysis to confirm the structural accuracy of the antimicrobial and anti-TB compounds **2a1, 2a3** and **2a20** that were tested Figs. 11–13. The molecular weight & purity of prepared analogs were confirmed from their mass spectrum.

3.10. Antimicrobial screening

In vitro experiments were carried out to assess the antibacterial properties of the newly synthesized derivatives. The tests involved bacterial strains from both Gram-positive and Gram-negative categories as well as fungal strains. Ciprofloxacin was used as the preferred treatment for bacterial infections, while Ketoconazole chosen for treating fungal infections. The screening results indicated that the derivatives **2a1, 2a3** and **2a20** showed notable activity Fig. 14.

3.11. In vitro anti TB screening

This research outlines the results of anti-tuberculosis screening on specific compounds: **2a1, 2a3** and **2a20**. The Microplate Alamar Blue

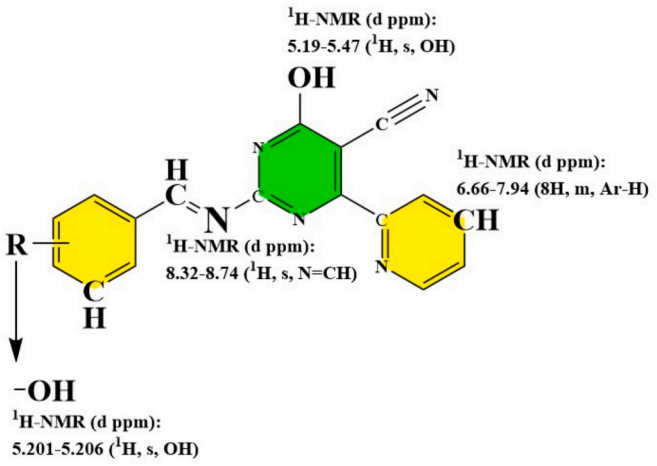

Fig. 12. ^{1}H NMR spectral assignment of the compound, highlighting key proton signals. Notable chemical shifts (δ, ppm) include 8.32–8.62 (1H, s, N═CH), 6.86–8.29 (8H, m, Ar—H), 5.19–5.32 (1H, s, OH), and 5.01–5.25 (1H, s, OH), confirming the presence of characteristic functional groups.

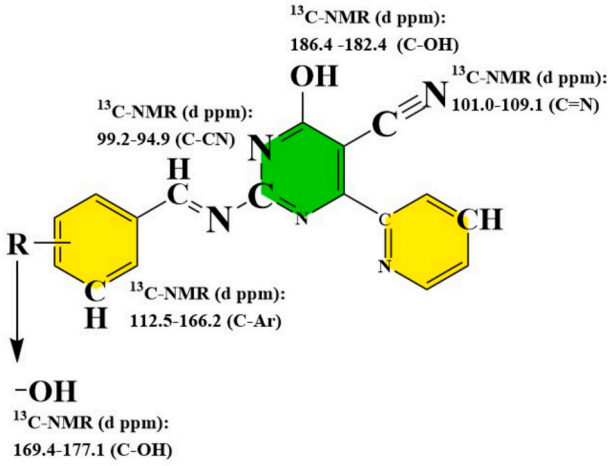

Fig. 13. ^{13}C NMR spectral assignments of the compound, displaying characteristic carbon shifts (δ, ppm). Key signals include C═N (114.0–115.3), N═CH (158.9–161.4), aromatic carbons (132.0–141.4), and carbonyl-related carbons (167.8–171.3, 175.5–182.4), confirming structural integrity.

Assay (MABA) method was utilized to evaluate the effects of these synthetic compounds on the growth of MTB*H37Ra* over a seven-day incubation period at 37 degrees Celsius. Six distinct concentrations were assessed: 0.97, 1.95, 3.90, 7.81, 15.62, and 31.25 μg/mL. The data indicate that compounds **2a1, 2a3** and **2a20** inhibited the MTB *H37Ra* strain across all tested concentrations. Specifically, compounds 2a1 and 2a3 were effective at a concentration of 3.90 μg/mL, while compound 2a20 showed efficacy at a lower concentration of 1.95 μg/mL. Notably, compound 2a20 demonstrated superior activity, identifying it as a highly effective analogue against tuberculosis microbial strains Fig. 15.

MTB is recognized for its thick and water-resistant cell wall, necessitating the use of potent anti-tuberculosis medications with high lipophilicity to penetrate this obstacle efficiently. Heterocyclic compounds are often recognized for their notable lipophilic characteristics, essential for biological activity and crossing cellular membranes. To study the impact of electronic effects on biological systems, we added electron-donating and electron-withdrawing groups to the pyridin-2-yl) pyrimidine-5-carbonitriles ring. By introducing bromine (an electron-withdrawing group) and hydroxy (an electron-donating group) at the ortho, meta, and para positions on this ring, we created several

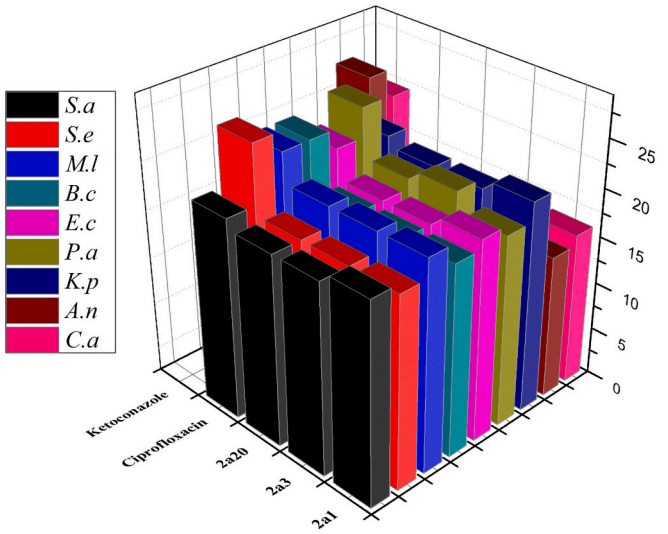

Fig. 14. 3D bar chart representing the antimicrobial activity of compounds **2a1, 2a3, and 2a20**, compared to ciprofloxacin and ketoconazole. The inhibition zones (mm) against various microbial strains are shown in different colors.

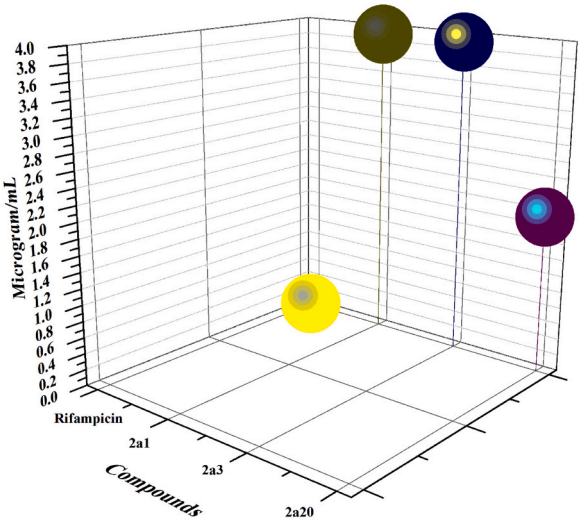

Fig. 15. 3D bubble plot representing the minimum inhibitory concentration (MIC) values (μg/mL) of compounds **2a1**, **2a3**, and **2a20**, compared to Rifampicin. The bubble size indicates relative MIC levels, with larger bubbles representing higher concentrations required for microbial inhibition.

analogues, specifically **2a1, 2a3** and **2a20**. The notable antibacterial efficacy of these compounds is likely due to the presence of these electron-modifying groups. Our findings indicate these groups enhance antibacterial potency.

The antibacterial activity values for compounds **2a1, 2a3** and **2a20**, along with the standard, are detailed in Table 10. Antimicrobial screenings demonstrated significant activity for halogen, heteroaromatic, hydroxy, and bromo compounds. Substituted pyrimidine compounds are of high interest in contemporary medicinal chemistry, in part because of their positive lipophilicity and excellent permeability through membranes. Data on the binding affinity (13.9 kcal mol1) of pyrimidines containing carbonitrile substituents to InhA, a proven target in antimicrobial and anti-TB treatment, were reported through molecular docking experiments. Good binding stability and specificity of the interaction 2a1, 2a3 and 2a20 scores similar or even higher than that of standard drug Ciprofloxacin. The study highlights fundamental

Table 10
Antimicrobial activity of pyrimidine-5-carbonitrile derivatives (**2a1, 2a3, 2a20**) against Gram-positive (*S.a, S.e, M.l, B.c*), Gram-negative (*E.c, P.a, K.p*), and fungal strains (*A.n, C.a*) at MIC 100 μg/mL. Ciprofloxacin and Ketoconazole were used as reference antibiotics. Zone of inhibition values (mm) are presented, with MIC values in parentheses.

Com	Zone of inhibition (MIC 100 μg/mL)								
	G^{+ve} *bacteria*				G^{-ve} *bacteria*			*Fungi*	
	S.a	*S.e*	*M.l*	*B.c*	*E.c*	*P.a*	*K.p*	*A.n*	*C.a*
2a1	21(10.6)	20(11.7)	22(10.8)	20(12.1)	21(12.7)	20(13.9)	22(12.6)	15(12.6)	16(11.9)
2a3	20 (10.9)	20(12.9)	22(11.6)	20(12.9)	20(13.5)	22(17.8)	21(13.6)	16(12.7)	16(15.6)
2a20	20(11.6)	20(13.4)	22(12.7)	20(13.1)	20(14.2)	21(17.6)	21(14.7)	16(13.1)	16(16.1)
Ciprofloxacin	21	27	25	25	23	26	22	–	–
Ketoconazole	–	–	–	–	–	–	–	25	22
DMF	–	–	–	–	–	–	–	–	–

S.a-Staphylococcus aureus, S.e-Staphylococcus epidermidis, M.l-Micrococcus luteus, Bacillus cereus, E.s-Escherichia coli, P.a-Pseudomonas aeruginosa, K.p-Klebsiella pneumonia, A.n-Aspergillus niger, C.a- Candida albicans.
Zone of inhibition in mm, MIC in μg/mL.

interactions, such as hydrogen bonding, π-π stacking, and hydrophobic interactions, vital for the binding of targets. Especially, the derivatives that have fluorinated substituents show better binding due to the electrostatic elements. The manuscript in fact compares the docking using standard drugs and potential therapeutic role of these new compounds. Moreover, the structure-activity relationship (SAR) analysis can help understand the electronic and lipophilic features associated with binding affinity to allow them to be effective antimicrobial agents. In Vitro efficacy is justified by experimental MIC values, thus paved 2a1, 2a3 and 2a20 as potential candidates in future drug development against resistant microbial strains though mathematics demonstrated that drug-likeness and computational data are very strong in support. The peculiar structure of pyrimidines presents a bright future of activity and physicochemical properties, and it is possible to obtain more effective derivatives of them in the framework of ongoing research. Table 11 represents the in vitro anti-TB screening outcomes of compounds **2a1, 2a3** and **2a20**, and the standard. The rational design of compounds **2a1, 2a3** and **2a20** targeted InhA enzyme inhibition for antimicrobial/anti-TB activity. Pyrimidine-5-carbonitrile scaffolds were selected for their established antimicrobial properties and structural similarity to nucleic acid bases. Strategic substitutions included electron-donating hydroxy groups (ortho/para positions in 2a1/2a3) and electron-withdrawing bromine (meta position in 2a20) to enhance lipophilicity, membrane penetration, and binding affinity while exploiting electronic effects for optimal biological activity against drug-resistant pathogens.

3.12. Analysis of SAR

The structural and bioactivity data for compounds **2a1, 2a3** and **2a20** present insufficient diversity to establish meaningful structure-activity relationships (SAR). With only three compounds featuring limited substitutional variations—hydroxy groups at different positions (2a1: para-OH, 2a3: ortho-OH) and a single halogen substitution (2a20: meta-Br)—the dataset lacks the breadth necessary for robust SAR analysis. The manuscript's SAR conclusions regarding electron-donating versus electron-withdrawing effects are overstated given this narrow structural scope. Additionally, the similar MIC values (0.25–2.0 μg/mL range) and comparable binding affinities (−8.572 to −16.497 kcal/mol) provide minimal differentiation to discern clear structure-activity trends. A comprehensive SAR study would require systematic exploration of multiple substitution patterns, positions, and functional groups across a larger compound series.

Table 11
Minimum inhibitory concentration (MIC) values of pyrimidine-5-carbonitrile derivatives (**2a1**, **2a3**, **2a20**) against *Mycobacterium tuberculosis*, compared with Rifampicin (control, 0.0095 μg/mL). **2a20** (3-Br) exhibited the lowest MIC (1.95 μg/mL), indicating the highest potency among tested compounds.

Com	R_1	MIC (μg/mL)
Rifampicin(control)		0.0095 μg/mL
2a1	4-OH	3.90 μg/mL
2a3	2-OH	3.90 μg/mL
2a20	3-Br	1.95 μg/mL

The data represents mean of three replicates.

To effectively bridge the structures, bioactivities, and molecular modeling for compounds **2a1, 2a3** and **2a20**, it is essential to integrate the findings from structural analysis, in vitro testing, and computational studies. The compounds were synthesized using Schiff base reactions, resulting in derivatives with various substituents on the pyrimidine ring, including hydroxy and bromo groups. These modifications were made to enhance lipophilicity and increase binding affinity, particularly targeting the InhA enzyme, which plays a crucial role in *Mycobacterium tuberculosis's* cell wall synthesis. The bioactivity results demonstrate that compounds **2a1, 2a3** and **2a20** exhibit potent antimicrobial and anti-TB activity, with minimum inhibitory concentrations (MIC) indicating their effectiveness against both Gram-positive and Gram-negative bacteria, as well as the MTB strain. These biological outcomes correlate with the computational results obtained from molecular docking studies. The compounds displayed strong binding affinities to InhA, supported by favorable interactions such as hydrogen bonding, π-π stacking, and hydrophobic interactions, as observed in the docking simulations. Furthermore, molecular dynamics (MD) simulations provided insights into the stability and dynamics of protein-ligand interactions, showing minimal fluctuations and stable binding, especially for compound 2a1. The inclusion of electronic effects, derived from the HOMO-LUMO analysis, further validates the compounds' potential for effective drug design by correlating their electronic properties with antimicrobial activity. This comprehensive approach positions these derivatives as promising candidates for further development as anti-TB agents.

4. Conclusion

Enhancing the activity can be achieved by making slight adjustments to the substituents the pyrimidine's core structure. The effectiveness of the compounds has been significantly boosted by the addition of hydroxy and bromo groups on the aromatic ring, as compared to other substituents. Based on the aforementioned data, our goal is to identify new candidates for the development of novel, specific, and less harmful anti-TB medications. Pyrimidine-5-Carbonitriles provides a strong rationale for the development of novel pyrimidine derivatives as possible antimicrobial agents. The study aims to combat the alarming problem of antimicrobial resistance by designing and assessing fused pyrimidine-5-carbonitrile derivatives for bacterial, fungal, and anti-tubercular activity. The authors demonstrate through their molecular docking studies that the compounds bind InhA, a crucial enzyme in fatty acid production in bacteria and that their binding affinities are

comparable or greater than Ciprofloxacin. The value of minimum inhibitory concentration (MIC) of major active compounds (**2a1, 2a3** and **2a20**) indicated that they possess strong antimicrobial action and can be considered as rational lead compounds. In addition, SAR studies show that lipophilic and electrophilic moieties enhance activity. Even though the in silico and in vitro findings indicate that to it is requisite to affirm efficacy and safety, new antimicrobial drugs are developed. The paper will be oriented towards the analysis of the intended results of electric effects and alterations of the core nucleus.

Authors contribution

Panneerselvam Theivendren contributed to the study's conception, design wrote the original manuscript. Xue Xia, Jian Shen, Jindong Dai, Koshika Arumuagam, Kanagaraj Rajalakshmi, Panneerselvam Theivendren, Selvaraj Muthusamy, Dongwei Zhu, Hao Dong Yuan performed synthesis and computational simulation and analyzed the data and proofread it. All the authors have read and approved the manuscript for submission.

CRediT authorship contribution statement

Xue Xia: Writing – review & editing, Writing – original draft, Funding acquisition, Data curation, Conceptualization. **Jian Shen:** Writing – review & editing, Writing – original draft, Visualization, Validation, Supervision. **Jindong Dai:** Writing – review & editing, Writing – original draft, Resources, Project administration, Methodology. **Koshika Arumuagam:** Writing – review & editing, Writing – original draft, Methodology, Investigation, Formal analysis. **Kanagaraj Rajalakshmi:** Writing – review & editing, Writing – original draft, Formal analysis, Data curation, Conceptualization. **Yuvaraj Dinakarkumar:** Writing – review & editing, Writing – original draft, Supervision, Software, Data curation. **Panneerselvam Theivendren:** Writing – review & editing, Writing – original draft, Methodology, Investigation, Data curation. **Selvaraj Muthusamy:** Writing – review & editing, Writing – original draft, Visualization, Validation, Supervision. **Dongwei Zhu:** Writing – review & editing, Writing – original draft, Visualization, Validation, Funding acquisition. **Haodong Yuan:** Writing – review & editing, Writing – original draft, Formal analysis, Data curation.

Funding

The authors sincerely thank the following funding sources: ① Zhang Jia Gang Science-Technology Supporting Plan of China (ZKYL2456) – Xue Xia ② National Natural Science Foundation of China (Grant No. 82202001) – Dongwei Zhu③ Postdoctoral Science Foundation of China (Grant No. 2024M761196) – Dongwei Zhu.

Declaration of competing interest

The authors declare that they have no known competing financial interests or personal relationships that could have appeared to influence the work reported in this paper.

Appendix A. Supplementary data

Supplementary data to this article can be found online at https://doi.org/10.1016/j.bioorg.2025.109167.

Data availability

No data was used for the research described in the article.

References

[1] A.P. Jena, V.V. Sarma, Biochemical, molecular, and computational techniques for the determination of virulence factors of ESKAPE pathogens, in: ESKAPE Pathogens: Detection, Mechanisms and Treatment Strategies, Springer, 2024, pp. 183–208, https://doi.org/10.1007/978-981-99-8799-3_6.
[2] J.-S. Lim, Y.-Y. Chai, W.-X. Ser, A. Van Haeren, Y.-H. Lim, T. Raja, J.-B. Foo, S. Hamzah, R. Sellappans, H.Y. Yow, Novel drug candidates against antibiotic-resistant microorganisms: A review, Iran. J. Basic Med. Sci. 27 (2024) 134, https://doi.org/10.22038/IJBMS.2023.71672.15593.
[3] Q. Luo, P. Lu, Y. Chen, P. Shen, B. Zheng, J. Ji, C. Ying, Z. Liu, Y. Xiao, ESKAPE in China: epidemiology and characteristics of antibiotic resistance, Emerg. Microbes Infect. (2024) 2317915, https://doi.org/10.1080/22221751.2024.2317915.
[4] S. Sajedi Moghaddam, S. Mamishi, B. Pourakbari, S. Mahmoudi, Bacterial etiology and antimicrobial resistance pattern of pediatric bloodstream infections: a 5-year experience in an Iranian referral hospital, BMC Infect. Dis. 24 (2024) 373, https://doi.org/10.1186/s12879-024-09260-w.
[5] B. Yu, Q. Liu, J. Sun, X. Fu, Y. Zhang, X. Sun, Phototherapy-based multifunctional nanoplatform for synergistic therapy against drug resistance bacteria: progress, advances and challenges, Chem. Eng. J. (2024) 150705, https://doi.org/10.1016/j.cej.2024.150705.
[6] A. Elfadadny, R.F. Ragab, M. AlHarbi, F. Badshah, E. Ibáñez-Arancibia, A. Farag, A. O. Hendawy, P.R. De los Ríos-Escalante, M. Aboubakr, S.A. Zakai, Antimicrobial resistance of Pseudomonas aeruginosa: navigating clinical impacts, current resistance trends, and innovations in breaking therapies, Front. Microbiol. 15 (2024) 1374466, https://doi.org/10.3389/fmicb.2024.1374466.
[7] P. Theivendren, S. Kunjiappan, Y.M. Hegde, S. Vellaichamy, M. Gopal, S. R. Dhramalingam, S. Kumar, Importance of protein kinase and its inhibitor: a review, in: Protein Kinases: Promising Targets for Anticancer Drug Research, IntechOpen, 2021, pp. 75–100, https://doi.org/10.5772/intechopen.98491.
[8] B. Kumar, J. Devi, A. Dubey, N. Tufail, D. Khurana, Thiosemicarbazone ligands based transition metal complexes: a multifaceted investigation of antituberculosis, anti-inflammatory, antibacterial, antifungal activities, and molecular docking, density functional theory, molecular electrostatic potential, absorption, distribution, metabolism, excretion, and toxicity studies, Appl. Organomet. Chem. (2024) e7345, https://doi.org/10.1002/aoc.7345.
[9] H. Yang, Z. Yao, K. Yang, C. Wang, M. Li, Y. Zhang, J. Yan, R. Lv, Y. Wang, A. Huang, Synthesis and antibacterial evaluation of novel psoralen derivatives against methicillin-resistant *Staphylococcus aureus* (MRSA), Chem. Biodivers. (2024) e202302048, https://doi.org/10.1002/cbdv.202302048.
[10] A.A. Oviatt, E.G. Gibson, J. Huang, K. Mattern, K.C. Neuman, P.F. Chan, N. Osheroff, Interactions between gepotidacin and *Escherichia coli* gyrase and topoisomerase IV: genetic and biochemical evidence for well-balanced dual-targeting, ACS Infect. Dis. (2024), https://doi.org/10.1021/acsinfecdis.3c00346.
[11] J.A. Collins, N. Osheroff, Gyrase and topoisomerase IV: recycling old targets for new antibacterials to combat fluoroquinolone resistance, ACS Infect. Dis. (2024), https://doi.org/10.1021/acsinfecdis.4c00128.
[12] A.A. Hamed, M.A. Ghareeb, N.R. Soliman, B. Bakchiche, S.K. Bardaweel, Insights into bioactive microbial natural products and drug discovery, Egypt. Pharm. J. 23 (2024) 1–15.
[13] K. Elumalai, A. Shanmugam, M. Devaraji, S. Srinivasan, Synthesis and molecular docking of pyrimidine derivatives as antibacterial agents, Carbon Resour. Convers. 7 (2024) 100222, https://doi.org/10.1016/j.crcon.2024.100222.
[14] A.H. Elwahy, H.F. Hammad, N.S. Ibrahim, H.A. Al-Shamiri, A.F. Darweesh, I. A. Abdelhamid, Synthesis and antibacterial activities of novel hybrid molecules based on benzothiazole, benzimidazole, benzoxazole, and pyrimidine derivatives, each connected to N-arylacetamide and benzoate groups, J. Mol. Struct. 1307 (2024) 137965, https://doi.org/10.1016/j.molstruc.2024.137965.
[15] K. Joshi, H. Pandya, A. Mahida, I. Modasiya, G. Dubal, Synthesis and antimicrobial activity of new dihydropyrazolo [1, 5-a] pyrimidine derivatives, Russ. J. Bioorg. Chem. 50 (2024) 304–312.
[16] H. Khalifa, S. Rasheed, J. Haupenthal, J. Herrmann, Y.M. Mandour, A.H. Abadi, M. Engel, R. Müller, A.K. Hirsch, M. Abdel-Halim, Development and evaluation of 2, 4-disubstituted-5-aryl pyrimidine derivatives as antibacterial agents, Arch. Pharm. (2024) e2300656, https://doi.org/10.1002/ardp.202300656.
[17] B. Nagaraju, M. Rajeswari, T. Mounika, G. Rajitha, G.S. Kumar, C.V. Rao, S. Maddila, Synthesis and anti-microbial studies of new series of 1, 2, 3, 4-tetrazole integrated thieno [2, 3-d] pyrimidine derivatives, J. Mol. Struct. 1295 (2024) 136485.
[18] J.R. Mandhadi, T. Panneerselvam, P. Parasuraman, Design, in silico modeling, toxicity study and synthesis of novel substituted semicarbazide derivatives of pyrimidine: an antitubercular agent, Curr. Bioact. Compd. 16 (2020) 294–301.
[19] C. Palanichamy, P. Pavadai, T. Panneerselvam, S. Arunachalam, E. Babkiewicz, S. Ram Kumar Pandian, K. Shanmugampillai Jeyarajaguru, D. Nayak Ammunje, S. Kannan, J. Chandrasekaran, Aphrodisiac performance of bioactive compounds from *Mimosa pudica* Linn.: in silico molecular docking and dynamics simulation approach, Molecules 27 (2022) 3799.
[20] T. Panneerselvam, V. Karthick, P.V. Kumar, Ali Synthesis and structure-activity relationship study of 2-(substituted benzylidene)-7-(4-fluorophenyl)-5-(furan-2-yl)-2H-thiazolo [3, 2-a] pyrimidin-3 (7H)-one derivatives as anticancer agents, Drug Dis. Therap. 6 (2012) 198–204.
[21] R.R. Rajeshkumar, B.K. Kumar, P. Parasuraman, T. Panneerselvam, K. Sundar, D. N. Ammunje, S.R.K. Pandian, S. Murugesan, S.J. Kabilan, S. Kunjiappan, Graph theoretical network analysis, in silico exploration, and validation of bioactive compounds from *Cynodon dactylon* as potential neuroprotective agents against α-synuclein, BioImpacts: BI 12 (2022) 487.

[22] G. Saravanan, T. Panneerselvam, S. Kunjiappan, P. Parasuraman, V. Alagarsamy, P. Udayakumar, M. Soundararajan, S.D. Joshi, S. Ramalingam, D.N. Ammunje, Graph theoretical analysis, in silico modeling, prediction of toxicity, metabolism and synthesis of novel 2-(methyl/phenyl)-3-(4-(5-substituted-1, 3, 4-oxadiazol-2-yl) phenyl) quinazolin-4 (3H)-ones as NMDA receptor inhibitor, Drug Dev. Res. 80 (2019) 368–385.

[23] S.R. Dixit, S.D. Joshi, V.H. Kulkarni, T. Panneerselvam, Synthesis and antitubercular activity of some novel 2, 5-dimethyl pyrrolyl benzohydrazide derivatives, Indian, J. Heterocyclic Chem. 27 (2017) 117–121.

[24] T. Panneerselvam, S. Kunjiappan, V. Alagarsamy, G. Saravanan, P. Parasuraman, Design, Optimization, Synthesis and AntiTB Screening of Benzimidazole Derivatives, Anti-Infective Agents 18, 2020, pp. 24–42, https://doi.org/10.2174/2211352517666190301144054.

[25] T. Panneerselvam, A. Sivakumar, S. Arumugam, S.D. Joshi, Design, docking analysis, identification, and synthesis of novel 3-(((substituted phenyl) amino) methyl)-2-methylquinazolin-4 (3H)-one compounds to fight tuberculosis, Drug Discov. Ther. 10 (2016) 188–194.

[26] P. Theivendren, A. Subramanian, S. Kunjiappan, S. Arunachalam, I. Murugan, S. Arumugam, Design, network analysis, in silico modeling and synthesis of biologically active thiazolo quinazoline scaffolds as anti-tubercular agent, Curr. Chem. Biol. 11 (2017) 140–149.